Supplementary Information

Surface-fill Hydrogel Attenuates the Oncogenic Signature of Complex Anatomical Surface Cancer in a Single Application

Poulami Majumder[1,a], Anand Singh[2,a], Ziqiu Wang[3], Kingshuk Dutta[4], Roma Pahwa[5], Chen Liang[1], Caroline Andrews[6], Nimit L. Patel[7], Junfeng Shi[1], Natalia de Val[3,b], Scott T. R. Walsh[1], Albert Byungyun Jeon[8], Baktiar Karim[8], Chuong D. Hoang[2*], Joel P. Schneider[1*]

[1] Chemical Biology Laboratory, National Cancer Institute, National Institutes of Health, building 376, Boyles St, Frederick, MD, United States

[2] Thoracic Surgery Branch, National Cancer Institute, National Institutes of Health, building 10-CRC, Bethesda, MD, Unites States

[3] Electron Microscopy Laboratory, Cancer Research Technology Program, Frederick National Laboratory for Cancer Research, Leidos Biomedical Research Inc, Frederick, MD, United States

[4] Department of Chemistry, University of Massachusetts Amherst, Amherst, MA, United States

[5] Urology Oncology Branch, National Cancer Institute, National Institutes of Health, building 10-CRC, Bethesda, MD, Unites States

[6] Cancer and Inflammation Program, Center for Cancer Research, National Cancer Institute, National Institutes of Health, Frederick, MD, United States

[7] Small Animal Imaging Program, Frederick National Laboratory for Cancer Research, Leidos Biomedical Research Inc., Frederick, MD, United States

[8] Leidos Biomedical Research, Inc., Molecular Histopathology Laboratory, Frederick National Laboratory for Cancer Research, Frederick, MD, United States

[a] These authors contributed equally to this work

[b] Center for Molecular Microscopy, Center for Cancer Research, National Cancer Institute, National Institutes of Health, Frederick, MD, Unites States

[*] Correspondence should be addressed to chuong.hoang@nih.gov or Joel.Schneider@nih.gov

Supplementary Methods

Syntheses of peptides

Fmoc-based solid phase peptide synthesis strategies were used employing RINK amide resin and HCTU activation. Dry resin-bound peptide was cleaved and side chain protecting groups were removed using a cleavage cocktail of TFA/thioanisole/ethanedithiol/anisole (90:5:3:2) for 2 h under Argon atmosphere. After diethyl ether precipitation, crude Peptides 1, 2, 3 and Cyclic-Peptide 1 were purified via RP-HPLC using a preparative Vydac C18 peptide column with a flow rate of 8 mL/min. Standard A (0.1% TFA in water) and Standard B (90% acetonitrile, 9.9% water, 0.1% TFA) were used as elutants. Purified peptide was lyophilized three times from water before using for hydrogelation. Peptide4 was similarly synthesized, and crude peptide was purified using a preparative PolymerX 10 µm RP-1 column with a flow rate of 8 mL/min. Standard C (20 mM ammonium bicarbonate) and Standard D (20 mM ammonium bicarbonate in 80:20 acetonitrile/water, v/v) were used as elutants. Analytical HPLC chromatograms and ESIMS of the purified peptides are provided in supplementary data (Supplementary Figure S1 and S2, respectively).

Nanoparticle fluorescence binding isotherms

For the fluorescence binding isotherms (Fig 2a), FAM (6-carboxyfluorescein, 5' end)-labeled chemically-modified double-stranded scrambled miRNA mimic was diluted in water and mixed with aqueous solutions of peptide in molar ratios ranging from 0.312 to 200 (peptide vs miRNA). Resulting suspensions were incubated 30 min at 37 ºC with constant agitation. Complexes were further diluted with HEPES (25 mM, pH 7.4) buffer to a final miRNA concentration of 30 nM. FAM-miRNA emission at 520 nm (ex, 490 nm) was recorded using a microplate reader (Tecan Infinite 200) with a band-pass filter of 20 nm. Fluorescence emission spectra of the FAM-labelled, scrambled miRNA alone and miRNA complexed with peptides 1-3 at a molar ratio of 50:1 (N:P = 10:1) were recorded on a PTI Fluorimeter and the data was collected using UV Probe 2.70 software (Shimadzu).

Circular Dichroism Spectroscopy

Equivolume aqueous solutions of Peptide 1 and scrambled miRNA (150 µL each) were mixed to afford Peptide 1 vs miRNA N:P ratios of 10:1, 5:1, 2:1, 1:1 and 0.5:1 where the final concentration of Peptide 1 was constant (32 µM) in each sample. Samples were equilibrated 30 min at 37 ºC with agitation and transferred to a quartz cell (pl=1 mm) and ellipticity immediately measured at

37 ºC, using 1 nm step size. Raw data was collected on a CD spectrophotometer (Jasco) using the software Spectra Manager version 2.14.06. The raw data was corrected for miRNA contribution and converted to mean residue ellipticity: $[\theta] = \theta_{obs}/(10*l*c*r)$ where θ_{obs} is the measured ellipticity (mdeg), l is the path length (0.1 cm), c is peptide concentration and r corresponds to the number of peptide amino acids.

Cell culture

National Cancer Institute-derived malignant pleural mesothelioma cell lines H2052 (catalog # CRL-5915) and H2373 (catalog # CRL-5943) were obtained from ATCC[1]. The cells were cultured as monolayers at 37°C and 5% CO2 in RPMI 1640, supplemented with 10% fetal bovine serum in presence of 1% penicillin and streptomycin solution. Low passage Epithelioid Mesothelioma cell line-52 (MB52) were obtained from MesobanK UK[2]. The normal mesothelial cell line NP4 were derived from normal human pleural membrane in the laboratory of Dr. Chuong D. Hoang at the National Cancer Institute, NIH, USA. The cell line was cultured and maintained as described previously.[3]

Confocal microscopy

For the intracellular nanoparticle localization studies, a 63× oil objective on a Zeiss LSM710 confocal microscope was used to visualize the cells and the data were collected using the software Zen 2012 SP5 (Zeiss). Lasers and band pass emission filters were used as: 405 nm laser; 390 nm–465 nm (Hoechst channel), 488 nm laser; 500 nm-550 nm (green channel) and 561 nm laser; 570 nm-600 nm (red channel). Planar and z stack images were processed using Fiji-ImageJ version 1.52p.

To determine the intracellular distribution of calcein in the presence or absence of Peptide 1/miRNA nanoparticles, cells were co-incubated with calcein and nanoparticles containing scrambled miRNA (unlabeled) complex for 4 h in optiMEM. The total miRNA concentration was 40 nM. Calcein was used at a final concentration of 100 µM. Cells were incubated with 2 µg/mL Hoechst 33342 for 30 min immediately before imaging. A 488-nm laser line and 500-550 nm bandpass filter was used to detect calcein fluorescence. The data were collected using the software Zen 2012 SP5 (Zeiss) and the images were processed using Fiji-ImageJ version 1.52p.

Mechanism of nanoparticle cellular uptake and cell entry efficiency

To determine the mechanism of cellular uptake of Peptide 1/miRNA nanoparticles, cells were incubated with a set of standard endocytosis inhibitors in serum-free media. In each case, cells were pre-incubated with inhibitors for 1 h followed by co-incubation with the nanoparticles for

another 1 h before analyzing miRNA fluorescence using flow cytometry. Median fluorescence intensity (MFI) for gated live cell population was determined for cells treated with each inhibitor and normalized with respect to the sample without inhibitor treatment. FlowJo version 10 was used to analyze flow cytometry data.

To determine miRNA cell entry efficiency of the nanoparticles as a function of N:P ratio, FAM-labeled miRNA was complexed with Peptide 1 in N:P ratios of 10:1, 5:1, 2:1 and 1:1. Nanoparticles were diluted with optiMEM (Thermo Fisher) to maintain a final miRNA concentration of 40 nM before adding into the cells. Cells were incubated with the nanoparticles for 1 h and processed as described in the Methods section (In vitro Transfection Efficiency) before analyzing by flow cytometry (flow cytometer: BD LSRII™, data acquisition: FACSDiva 8.0.1; data analysis: FlowJo version 10).

Evaluation of gene silencing with qPCR

To determine the efficacy of Peptide 1/miRNA nanoparticles for functional delivery of miRNA into mesothelioma cells, miRNA-215 or miRNA-206 (Thermo Fisher) was complexed with Peptide 1 to form 10:1 (N:P) nanoparticles following the procedure described in the Methods section. A scrambled miRNA with no known sequence similarity to human genes (Thermo Fisher) was used to prepare similar nanoparticles as a negative control. Sequences of all miRNAs used are described in Table S1. To compare the gene silencing efficacy of the nanoparticles with commercially available transfection reagent, Lipofectamine RNAiMAX was complexed with an equivalent amount of miRNA following the manufacturer's protocol. 2×10^5 cells were seeded on 6 well plates 24 h before treatment and allowed to grow under normal culture conditions. Cells were incubated with complexes diluted with optiMEM (final miRNA concentration 40 nM) for 4 h, washed and incubated with fresh complete media for another 44 h. Total RNA was isolated from cells using TRIzol™ (Thermo Fisher) following standard protocol. RNA concentration and purity were determined by Nanodrop. cDNA from each treatment group was synthesized using a High-Capacity cDNA Reverse Transcription Kit (Applied Biosystems) and mRNA expression for target genes (CDC7, LMNB2, MDM2 and MAD2L1 for miRNA-215; MET, KRAS, CCND1 and CDK4 for miRNA-206) were measured on QuantStudio 6 Flex Real-Time PCR System (Applied Biosystems) using corresponding TAQ-MAN probes (details in Table S2). Expression levels of target genes in cells treated with Peptide 1 or Lipofectamine complexes of miRNA-215, miRNA-206 and scrambled miRNA were normalized to the housekeeping gene β-actin. Data in miRNA-215 and miRNA-206-treated groups are expressed as a fold change with respect to the expression level of the corresponding gene in the samples treated with scrambled miRNA, delivered with the corresponding transfection agent.

To compare target gene silencing efficacy between 10:1 (N:P) and 1:1 (N:P) nanoparticles, cells were treated with each set in a separate experiment and were processed as described above, while maintaining 40 nM final miRNA concentration for each type of nanoparticles.

The dependence of endosomal escape on the target gene silencing efficacy of the 10:1 particles was determined by treating cells with Bafilomycin A1 (Sigma), a vacuolar ATPase inhibitor for 1 h before addition of the nanoparticles, followed by co-incubation with the nanoparticles for 4 h. Bafilomycin concentration was maintained at 50 nM. Cells were incubated with nanoparticles diluted with optiMEM to keep the final miRNA concentration at 40 nM. Cells were washed after 4 h and incubated with fresh complete media for another 20 h. Processing steps were similar as described above for RNA extraction and qPCR-based quantification of the target genes.

Cell viability assay

To determine the biocompatibility of Peptide 1/miRNA nanoparticles, 1×10^4 H2052 cells were seeded on 96 well plates 24 h before transfection. Nanoparticles prepared with scrambled miRNA were incubated with cells in optiMEM to maintain a final miRNA concentration of 40 nM and cell viability was determined 4 h post-addition of nanoparticles.10 µL of MTT solution (5 mg/mL in PBS) was added and cells were incubated for 4 h at 37 ºC. The supernatant was discarded and 100 µL of DMSO was added to dissolve the purple formazan crystals. Absorbance was measured at 550 nm using a UV plate reader (Biotek, Winooski, VT). The absorbance of each sample was subtracted from a blank (without MTT solution), and percent viability was calculated using the equation: $(\text{Absorbance}^{\text{treated}}/\text{Absorbance}^{\text{untreated}}) \times 100$.

An LDH assay kit (Roche) was used to determine any possible cytotoxicity of Peptide 1/miRNA nanoparticles. Cell supernatant was taken out after 4 h of treatment with the nanoparticles and a reaction mixture containing diaphorase/NAD+/iodotetrazolium chloride/sodium lactate was added following manufacturer's instructions to detect any released LDH (Lactate Dehydrogenase). Triton X-100 at a final concentration of 1% (v/v) was used as the positive cell lysis control and untreated cells represent the negative control. Absorbance was measured at 490 nm after 5 minutes of incubation at 37 ºC. Cytotoxicity was calculated using the equation:

$(\text{Absorbance}^{\text{treated}}-\text{Absorbance}^{\text{low control}}/\text{Absorbance}^{\text{high control}}-\text{Absorbance}^{\text{low control}}) \times 100$.

To evaluate the anti-proliferative ability of intracellularly delivered miRNA-215 and miRNA-206, H2052 cells were plated at a density of 2.5×10^3 a day before transfection and were similarly treated. Each sample was incubated for 4 h in optiMEM with particles delivering a total of 40 nM final miRNA concentration, washed and incubated with complete media for 3 days or 5 days. Cell viability was determined using CellTiter 96® Aqueous One Solution Cell Proliferation Assay (Promega) according to the manufacturer's instructions by measuring absorbance at 490 nm.

Clonogenicity assay

The clonogenic potential of cells transfected with Peptide 1/miRNA-215 or Peptide 1/miRNA-206 nanoparticles were determined using a 2D colony foci formation assay and anchorage independent 3D soft agar colony formation assay. 2.5×10^3 H2052 cells were seeded on 96 well plate 24 h before transfection and treated with the nanoparticles. Each sample was incubated for 4 h in optiMEM with 40 nM final miRNA concentration, washed and incubated with complete media for overnight. Cells were trypsinized, counted and 1×10^3 transfected cells were seeded on 12 well plate. Cells were allowed to adhere and proliferate under normal culture conditions for 2 weeks. Colonies were stained with 0.5 wt% crystal violet and imaged.

To determine anchorage-independent cell growth, soft agar assay was performed in 12 well plates with pre-transfected cells. Briefly, H2052 cells were first seeded and treated in 96 well plate following the protocol described above. Before transferring transfected cells into 12 well plate, wells were pre-coated with 0.5 wt% agarose and were allowed to solidify at room temperature. Transfected cells were trypsinized, counted and 1×10^3 cells resuspended in complete media containing 0.4 wt% agarose and seeded on top of agarose base (0.5 wt%). Cells were allowed to grow in 3D for 6 weeks under normal culture conditions, imaged using an Olympus IX51 Microscope and SPOT Basic (Version 4.6) imaging software and counted.

***In vitro* release of miRNA from SFH**

SFHs were prepared in cylindrical glass vials as described previously and had only the top surface exposed to buffer for the release. Each sample contained a total of 1 µg of FAM-labeled scrambled miRNA. 1 mL HBS (pH 7.4) was added on top of the gels and the vials were agitated at 37 ºC (50 rpm). At scheduled time points, the entire supernatant was removed and replaced with 1 mL fresh HBS. To ensure miRNA dissociation from released nanoparticles, Heparin (Heparin sodium salt from porcine intestinal mucosa, Grade I-A) solution was added to the removed supernatant at each time point at a final concentration of 10 µg/mL. Concentrations of released miRNA in the supernatant were determined by measuring fluorescence of the removed aliquot. FAM-miRNA was excited at 490 nm and emission intensity at 520 nm was recorded on a PTI fluorimeter and

the data was collected using UV Probe 2.70 software (Shimadzu). miRNA concentration was calculated based on a standard curve.

Aggregation assay for nanoparticles encapsulated within SFH

Nanoparticles were prepared by incubating an increasing amount of scrambled miRNA (5, 10, 15 and 20 µg) with Peptide 1 while maintaining an N:P ratio of 10:1 across compositions. Concentrations of Peptide 1 and miRNA stock solutions were adjusted to accommodate the required amount of miRNA within a fixed volume of 25 µL. Nanoparticle suspensions were mixed with 25 µL of ice-chilled 2X HBS followed by the addition of 50 µL of 1 wt% solution of Peptide 3 in chilled 25 mM HEPES (pH 7.4). 90 µL of each suspension was immediately transferred into a clear, flat-bottom 96-well UV-transparent plate which was carefully sealed to avoid air-drying. The plate was incubated at 37 ºC for 1 h and absorbance at 660 nm was recorded using a SpectraMax iD5 Multi-Mode Microplate Reader (Molecular Devices) which marked the data point of d0. Subsequent measurements were performed at d1, d2, d3 and d7. %Transmittance was derived from the absorbance values using the equation: log(%T) = 2 − Absorbance. %Transmittance values for each set of SFH were normalized against the corresponding values at d0.

Thickness determination of sprayed SFH

To measure the thickness of SFH after spray delivery, SFH (0.2 mL) was prepared within the gravity fluid cup of the airbrush as described in the Methods section. The sample was then allowed to equilibrate for two days at 37 ºC. This was followed by addition of 0.5 mL of calcein (0.2 mg/mL in water) on top of the gel. SFH was washed after incubating with calcein for 2-3 days. SFH was then sprayed (as described above) onto the wells of a 8-well chamber slide. The gel samples were visualized on a Zeiss LSM710 confocal microscope using 488 nm excitation laser and 500 nm-550 nm band-pass emission filter. Images were collected at multiple heights by acquiring xy slices from a position below the glass slide up to that above the gel. The slices were combined to generate a z-stacked image. Lengths along Z-direction were measured across 5 locations of the slices using ImageJ to calculate the thickness of the sprayed gel.

Cellular transfection and gene silencing with nanoparticles released from SFH

To determine the transfection ability of nanoparticles released from SFH, gels containing 0.5 wt% Peptide 3 were loaded with nanoparticles consisting of FAM-labeled scrambled miRNA. 1 mL of optiMEM was added on top of the SFH and the vials were agitated at 37 ºC (50 rpm) for 24 h. Release supernatant was collected and incubated with H2052 cells for 4 h. Cells were seeded 4 days before treatment at a density of 5×10^4 on glass bottom petridishes. Cells were washed,

transferred to complete media and stained with 2 µg/mL Hoechst 33342 for 30 min before imaging with an LSM710 confocal microscope.

To evaluate the gene silencing ability of released nanoparticles, SFHs were separately loaded with nanoparticles containing miRNA-215 and scrambled miRNA. 1 mL of optiMEM was added on top of the SFH and the vials were agitated at 37 ºC (50 rpm) for 24 h. Released supernatant was collected and incubated with H2052 cells for 4 h. Cells were seeded 24 h before treatment at a density of 2×10^5 per well of 6 well plates. Media was replaced with fresh complete media after 4 h and cells were allowed to grow for another 44 h. Total RNA was isolated and gene expression was analyzed using qPCR following the previously described protocol.

To determine the transfection ability of miRNA released from the hydrogel of Peptide 4, 1 mL of optiMEM was added on top of the gel and the vials were agitated at 37 ºC (50 rpm) for 4 h. Released supernatant was collected and incubated with H2052 cells for 4 h. Confocal microscopy images were acquired as described above.

In vivo studies

For the experiments described in the main text methods and here in the Supplemental Information, athymic nu/nu mice (female, 6-8 weeks old), NOD.Cg-PrkdcscidIl2rgtm1Wjl/SzJ (NSG) mice (male or female, 6-12 weeks old) and C57BL/6J mice (female, 5-7 weeks old) were used for this study. All animals were housed in a specific pathogen-free environment at ambient temperature (24 ± 2 °c), air humidity 40 - 70% and 12 h dark/12 h light cycle. All animal studies were approved by the Institutional Animal Care Committee, NIH. Frederick National Laboratory is accredited by AAALAC International and follows the Public Health Service Policy for the Care and Use of Laboratory Animals. Animal care was provided in accordance with the procedures outlined in the “Guide for Care and Use of Laboratory Animals” (National Research Council; 2011; National Academies Press; Washington, D.C.).

In vivo release of miRNA nanoparticles from SFH

For *in vivo* studies, purified Peptide 1 and Peptide 3 were tested for endotoxin levels using a LAL chromogenic endotoxin quantification kit (Pierce, Rockford, IL). Endotoxin levels were regularly found to be below the detection limit. For the *in vivo* miRNA release study, SFH containing 0.5 wt% and 1 wt% Peptide 3 were loaded with nanoparticles composed of 10 µg of cy3-labeled scrambled miRNA (Thermo Fisher). Each sample was transferred to sterile 27G syringes and allowed to undergo gelation for 24 h at 37 ºC. 100 µL of hydrogel was subcutaneously administered to each athymic nu/nu mouse (n = 3) on the lower back. An equivalent amount of naked miRNA solution in HBS was similarly administered as a control (n = 2).

Optical imaging

Cy3 fluorescence was longitudinally monitored (1 h, 5 h, day 2, 3, 7, 9, 11, 14, 18, 21 and 24) employing an IVIS spectrum imager (PerkinElmer Inc., Waltham, MA). Imager specific Living Image software (version 4.3.1) was used for image acquisition and analysis. Mice body temperatures were kept constant at 37ºC during the procedure with a heated pad located under the anesthesia induction chamber, imaging table, and post procedure recovery cage all maintained at 37ºC. All mice were anesthetized in the induction chamber with 3% isoflurane with filtered (0.2 µm) air at 1 liter/minute flow rate for 3-4 minutes and then modified for imaging to 2% with O_2 as a carrier with a flow rate 1 liter/minute. Static 2D images were acquired in prone position with the following parameters: excitation filter 570 ± 15 nm, emission filter 620 ± 10 nm, f/stop 2, medium binning (8X8) and auto exposure (typically 1-60 seconds). Circular regions of interest (ROI) were drawn on the injection site to evaluate the *in vivo* release of the miRNA (total radiance efficiency (photons/second/cm^2/steradian/mW).

Ultrasound imaging

B-mode ultrasound imaging was performed using a Vevo2100 scanner (FUJIFILM VisualSonics Inc., Toronto, CA) to assess hydrogel degradation (day 1, 2, 3, 5, 7, 9, 11, 14 and 18). To acquire a 3D volume, a stack of 2D B-mode images were captured using the MS 550S (40 MHz) linear array transducer with a step size of 0.076 mm while keeping the animal in the prone position. Animal body temperature was maintained at 37ºC and the same anesthesia protocol was followed as described in the optical imaging section. Hydrogel volume (cubic millimeter) was measured using the parallel contour algorithm within the Vevo LAB software 1.7.1 (FUJIFILM VisualSonics Inc., Toronto, CA) at each timepoint.

H & E staining

After ultrasound imaging at specific time points, mice were euthanized by CO_2 asphyxiation and the skin and subcutis were collected from the hydrogel injection site. Collected tissues were fixed in 10% neutral buffered formalin for 24 h and transferred to 70% ethanol. Sections of 5 µm thickness were generated from paraffin-embedded tissues which were then stained with hematoxylin and eosin for histopathological examination by a board-certified veterinary pathologist.

Safety profile assessment in immunocompetent mice

C57BL/6J mice were subcutaneously administered with 200 µL of SFH formulations. Mice were euthanized 3, 14, and 31 days after gel implantation and body weights were recorded. Major organs (brain, heart, kidney, liver, lung, and spleen) were weighed at the time of collection. Brain,

spinal cord, ovary, lung, kidneys, liver, heart, endocrine glands, thymus, spleen, lymph nodes, stomach, small and large intestine, femur and vertebrae, and skin were fixed in 10% buffered formalin, 5 µm sections were prepared, stained with H&E for histopathological analysis.

Blood examination and serum chemistry

31 days after SFH implantation, blood was taken and both serum and blood were analyzed. Blood (20 µL) was analyzed using Genesis™ Veterinary Hematology Analyzers. The blood exam included total red blood cells (RBC), total white blood cells (WBC), and differential WBC counts. Thrombin, partial thrombin, hemoglobin, packed cell volume, mean corpuscular hemoglobulin (MCH), and mean corpuscular hemoglobulin concentration (MCHC) were also measured. Serum chemistry (100 µL) was analyzed using VetScan VS2® Portable Chemistry Analyzer, for liver, kidney, and pancreas functions as well as muscle changes.

Immunohistochemical staining

5 µm-thick serial sections from skin and subcutaneous area including hydrogel region were prepared. Staining for CD3, CD45R/B220, Ly6G, and F4/80 markers were performed on LeicaBiosystems' BondRX autostainer. Following antigen retrieval with citrate buffer (Bond Epitope Retrieval 1), sections were incubated with CD3 (BioRad #MCA1477) at a dilution of 1:100 for 60 min, CD45R (BD Bioscience #553086) at a dilution of 1:400 for 30 min, and Ly6G (Origene #DM3589P) at 1:100 dilution for 30 min. Proteinase K (DAKO) was applied to sections for 5 min at room temperature prior to incubation with F4/80 (eBioscience #14-4801) at a dilution of 1:200 for 60 min. Stains were completed with biotinylated rabbit anti-rat IgG secondary antibody moused adsorbed (H+L) (Vector Laboratories #BA-4001) at a diluted of 1:100 and the Bond Polymer Refine Detection Kit (LeicaBiosystems #DS9800) with omission of the Post-Primary Reagent. CD45 staining was performed manually. Following antigen retrieval with citrate buffer (Vector Labs) in a Decloaking Chamber (Biocare), sections were blocked with normal rabbit serum then incubated overnight at room temperature with CD45 (BD Bioscience #550539) at a dilution of 1:100. Staining was completed with biotinylated rabbit anti-rat IgG secondary antibody moused adsorbed (H+L) (Vector Laboratories #BA-4001) at a diluted of 1:100, ABC Elite, and DAB (all from Vector Labs). Isotype control reagents were used in place of the primary antibodies for negative controls.

Image analysis

H&E slides and IHC slides were scanned at 20X using an Aperio AT2 scanner (Leica Biosystems, Buffalo Grove, IL) into whole slide digital images. All image analysis was performed using HALO imaging analysis software (Indica Labs, Corrales, NM). Slides were then thoroughly annotated by

a Board-certified pathologist who was blinded to the status of the groups of mice. The gel area was annotated and surrounding tissues such as connective tissue were excluded from the analysis. Image analysis was performed using cytonuclear algorithm in HALO version 3.2 to determine percent positive cells.

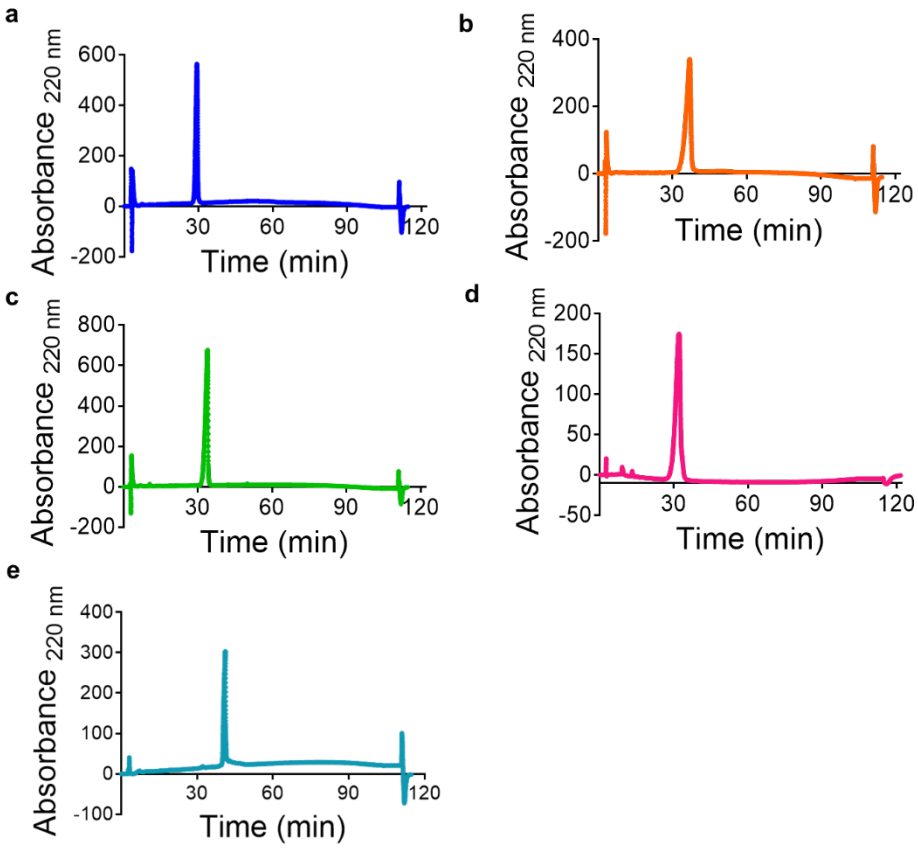

Figure S1. Analytical HPLC of purified peptides used in the study. **a**, Peptide 1 **b**, Peptide 2 **c**, Peptide 3, **d**, Peptide 4 and **e**, Cyclic-Peptide 1. Peptides 1, 2, 3 and Cyclic-Peptide 1 were analyzed using a Vydac C18 peptide/protein column and eluted using 0%-100% of Standard B (details in Methods section) over 100 min. at 40 °C. Peptide 4 was analyzed using a PolymerX 10 µm RP-1 column and eluted with 0% - 100% of Standard D (details in Methods section) over 100 min. at 40 °C.

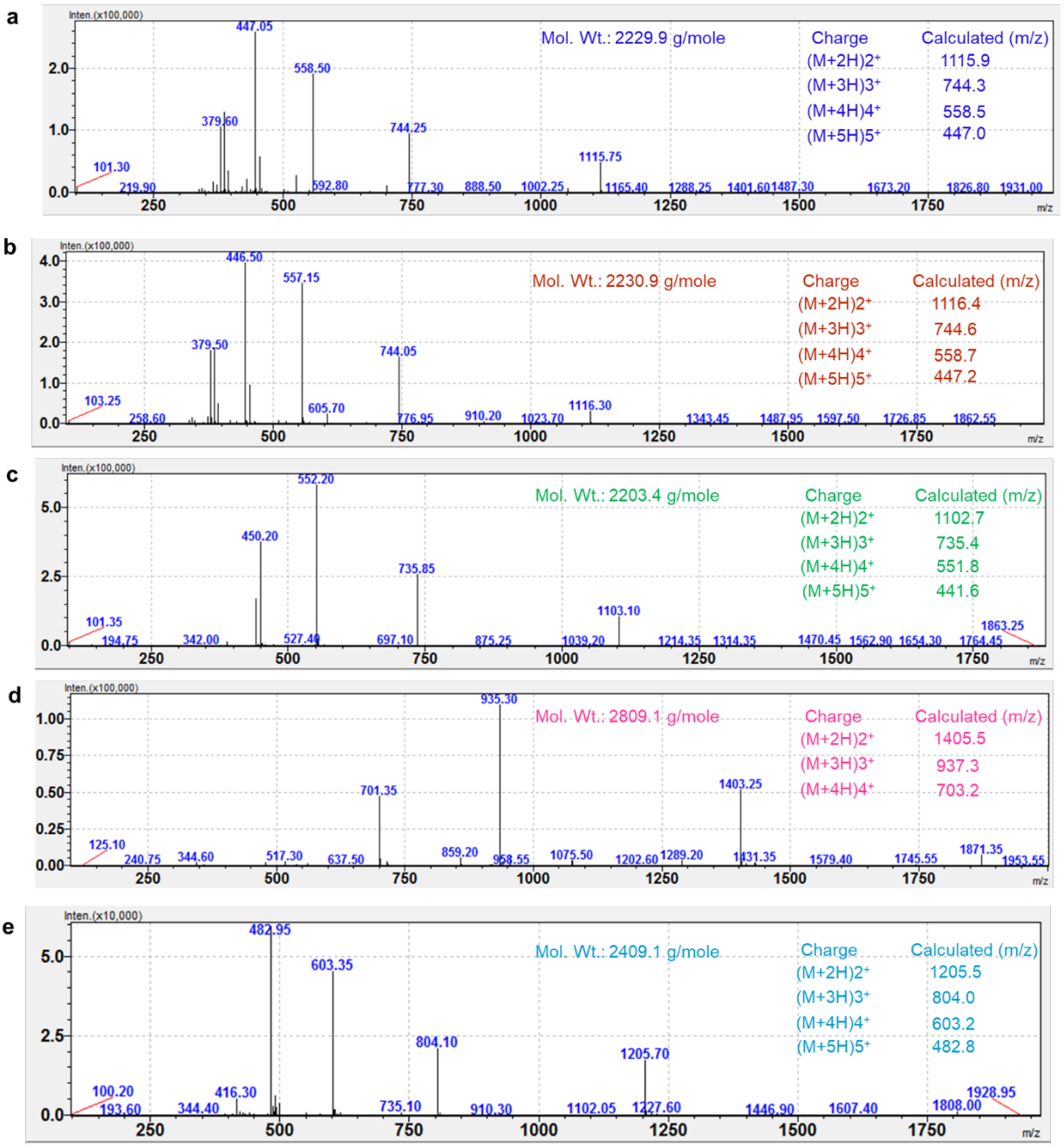

Figure S2. ESIMS of purified peptides used in the study. **a**, Peptide 1 **b**, Peptide 2 **c**, Peptide 3, **d**, Peptide 4 and **e**, Cyclic-Peptide 1.

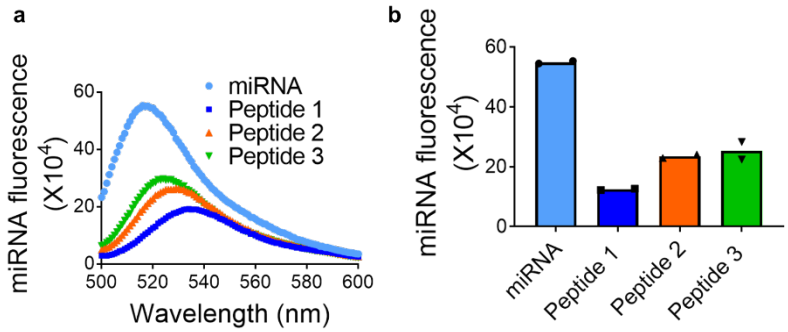

Figure S3. Representative fluorescence emission spectra corresponding to Figure 2a. **a**, Fluorescence of FAM-labelled, scrambled miRNA alone and complexed with peptides 1-3 at a molar ratio of 50:1 (charge ratio N:P = 10:1), the ultimate ratio used to formulate nanoparticles in subsequent studies. Excitation wavelength was 490 nm and emission was measured at 520 nm. **b**, Quantification of fluorescence spectra in panel (a), Data are shown for n = 2 independent samples.

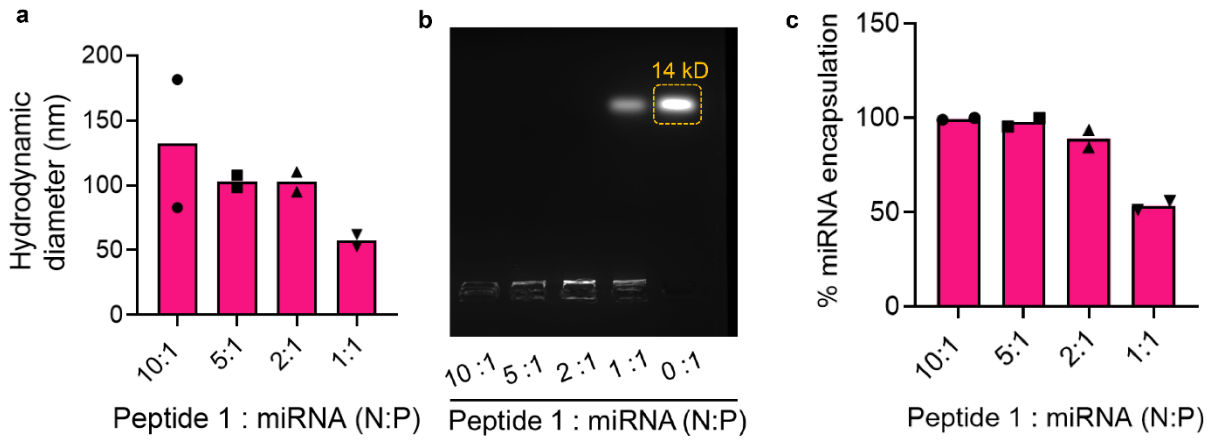

Figure S4. Size distribution profiles and miRNA encapsulation efficiency of Peptide 1/miRNA nanoparticles. **a**, Hydrodynamic diameters of nanoparticles at different N:P ratios of Peptide 1 and miRNA, as determined using DLS. Number-weighted size distribution data are shown for n = 2 independent samples. **b**, Agarose gel retardation assay of the nanoparticles at indicated N:P ratios. Electrophoretic pattern of uncomplexed miRNA (molecular weight 14 kD, 0:1; peptide 1:miRNA (N:P)) is shown on the rightmost lane and serves as control and molecular weight marker. miRNA bands were visible after ethidium bromide staining. Uncropped Gel (Figure S26e). Image is representative of 2 independent experiments. **c**, For each set of nanoparticles, the band at the locations corresponding to that for the naked uncomplexed miRNA was quantified for intensity using ImageJ and normalized against the intensity of the control uncomplexed miRNA band of known concentration to calculate miRNA encapsulation efficiency. Data are shown for n = 2 independent experiments.

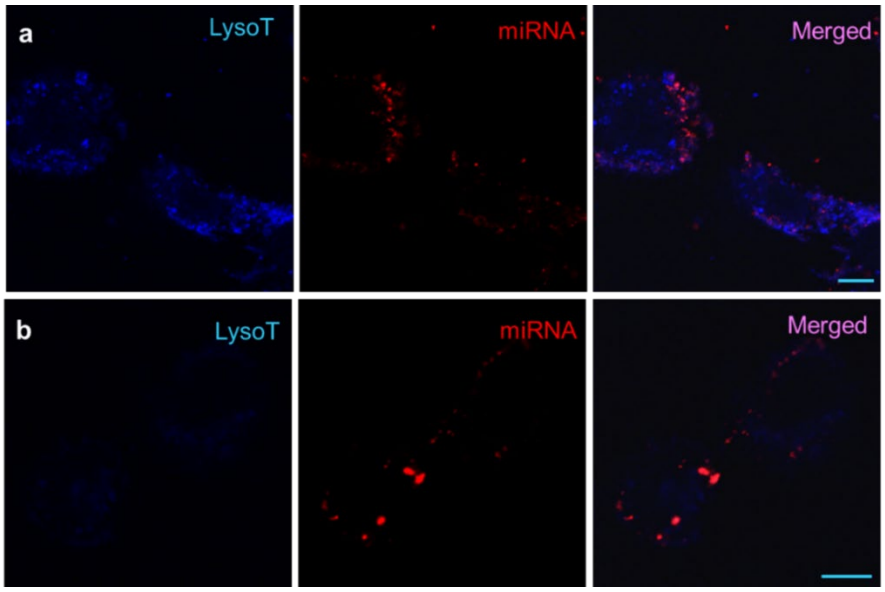

Figure S5. Intracellular distribution of Peptide 1/miRNA nanoparticles. Confocal microscopy of live H2052 cells treated for 30 min (**a**) and 4 h (**b**) with nanoparticles containing cy3miRNA (red) formulated at an N:P ratio of 10:1. Co-localization of cy3miRNA and the late endosome/lysosome marker lysotracker blue (LysoT) was determined at each time point. Final miRNA concentration is 40 nM in each panel. Scale bar 10 μm. Data are representative of 2 independent experiments.

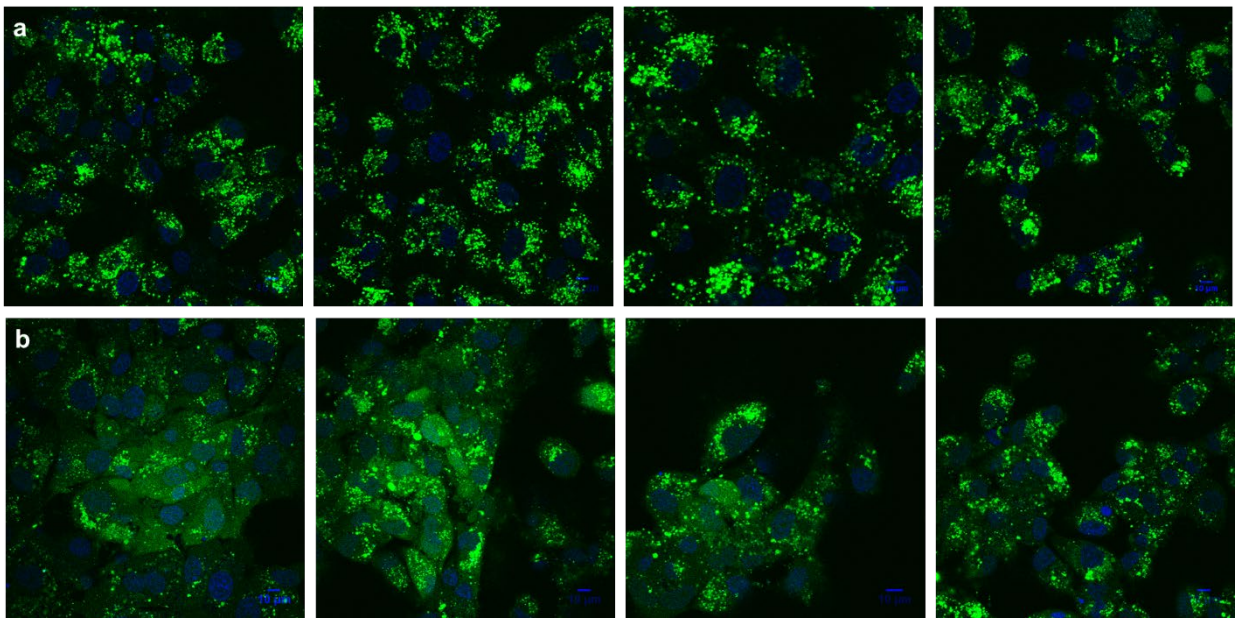

Figure S6. **Calcein release assay shows that Peptide 1/miRNA nanoparticles facilitate endosomal escape.** a, four representative images showing that calcein alone incubated with cells is endocytosed and remains in endosomes after 4h. b, four representative images showing that a significant portion of calcein co-incubated with Peptide 1/miRNA particles (N:P, 10:1) is released from endosomes at 4 h. Scale bar on each image is 10 μm. Data in (a,b) are representative of 3 independent experiments.

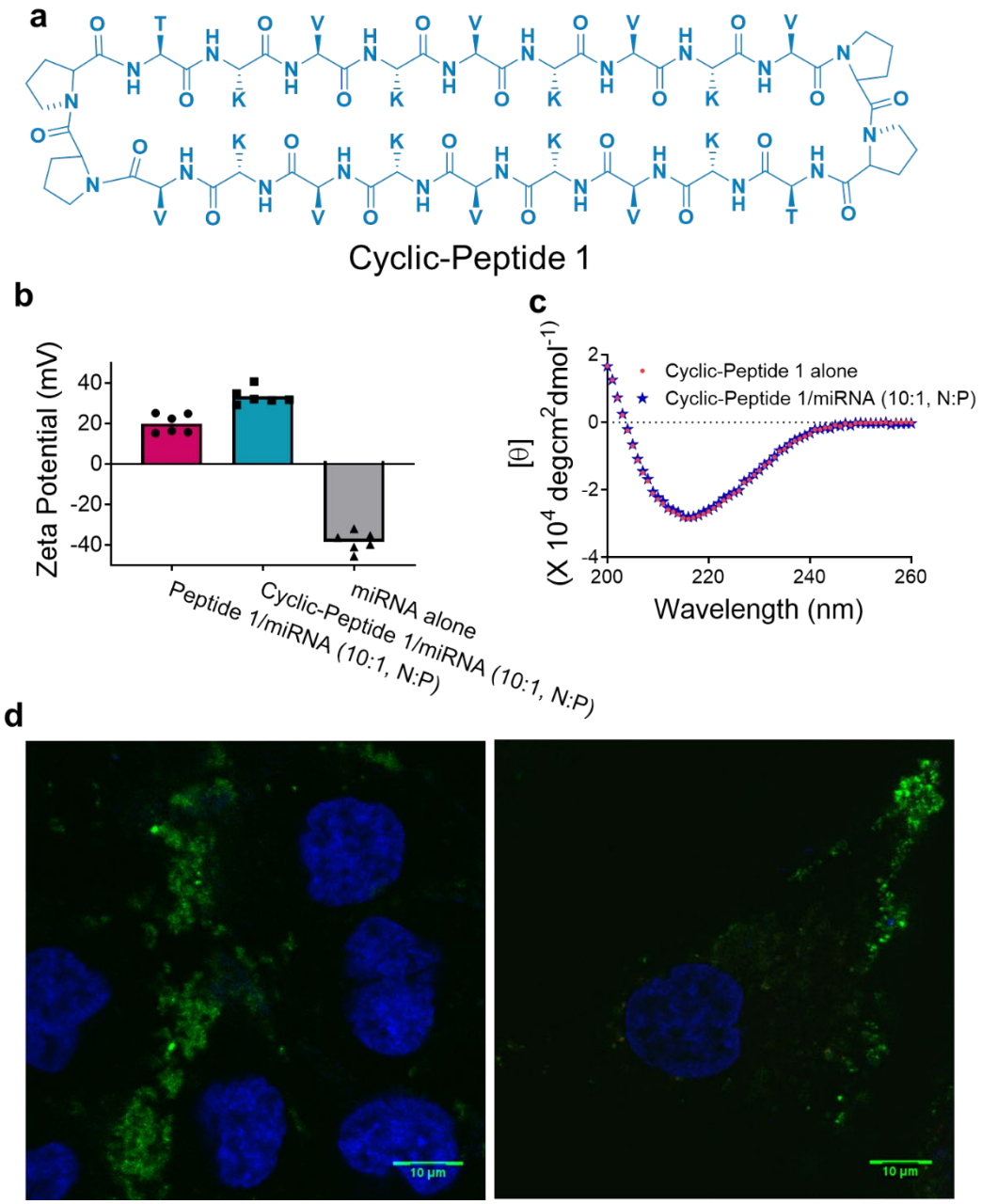

Figure S7. Folded Cyclic-peptide 1/miRNA nanoparticles partition to the cell surface but are unable to internalize into H2052 cells. a, Sequence of Cyclic-peptide 1. **b**, Zeta potential of nanoparticles composed of scrambled miRNA and Peptide 1 or Cyclic-peptide 1 compared to free miRNA. Data are shown for n = 6 measurements over 2 independent experiments. **c**, CD spectroscopy of Cyclic-peptide 1 alone and complexed to scrambled miRNA within nanoparticles. **d**, Confocal microscopy images of live cells treated for 30 min with particles comprised of scrambled miRNA and Cyclic-peptide 1 at a final miRNA concentration of 40 nM. Nanoparticles composed of cyclic-peptide 1 and scrambled miRNA accumulate between cells and at their surfaces, but very little enters. Data are representative of 2 independent experiments.

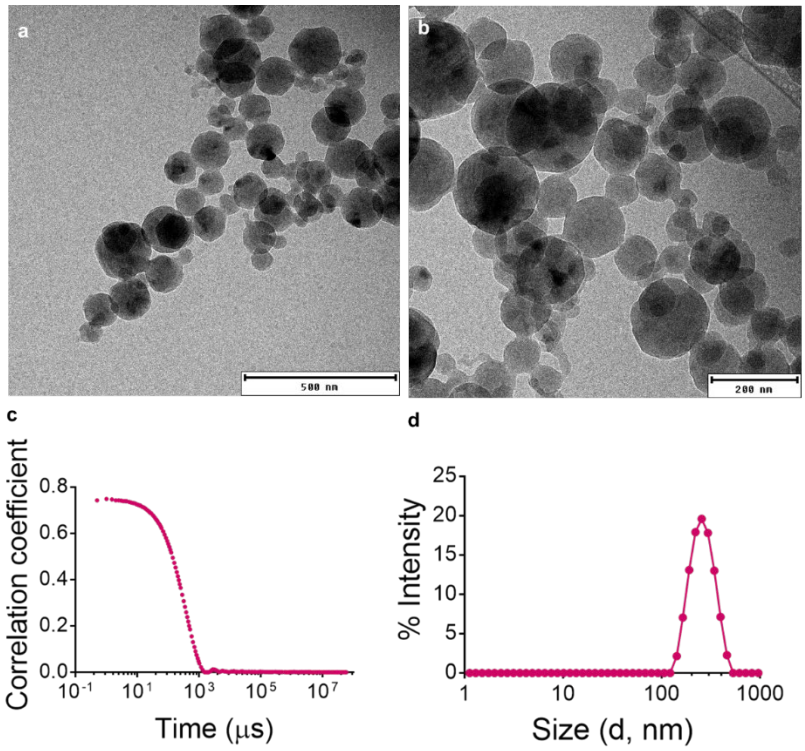

Figure S8. Morphology and size distribution of 10:1 (N:P) particles. a & b, Representative cryo-electron micrographs of particles. Data is representative of 2 independent experiments. **c**, DLS-derived correlogram of particles along with the associated size distribution histogram, **d**.

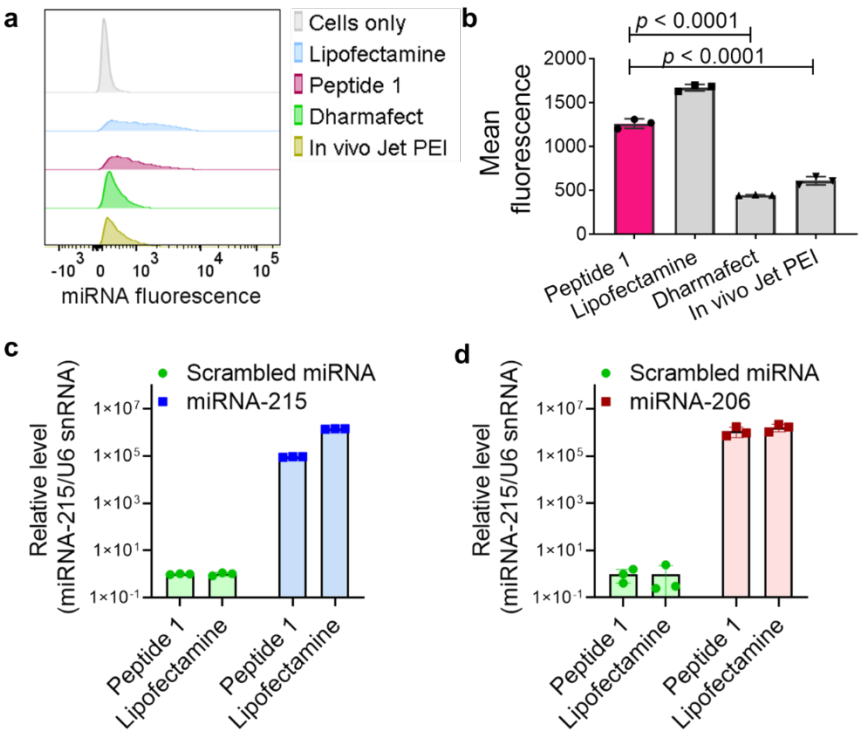

Figure S9. Comparing cellular transfection facilitated by 10:1 (N:P) particles versus other agents. a, Flow cytometric histograms for H2052 cell transfection. Representative of 2 independent experiments each measured over 3 independent samples. **b**, Mean fluorescence of cells transfected with particles versus other agents 1h post-exposure. Data = mean ± SD, n = 3 independent samples, representative of 2 independent experiments. Ordinary one-way ANOVA & Dunnett's multiple comparison test. **c**, Relative levels of miRNA-215 in H2052 cells after transfection with Lipofectamine and 10:1 (N:P) particles each carrying miRNA-215. Data = mean ± SD, n = 3 independent experiments. **d**, Relative levels of miRNA-206 in H2052 cells after transfection with Lipofectamine and 10:1 (N:P) particles each carrying miRNA-206. miRNA levels were normalized to U6 snRNA. Data = mean ± SD, n = 3 independent experiments.

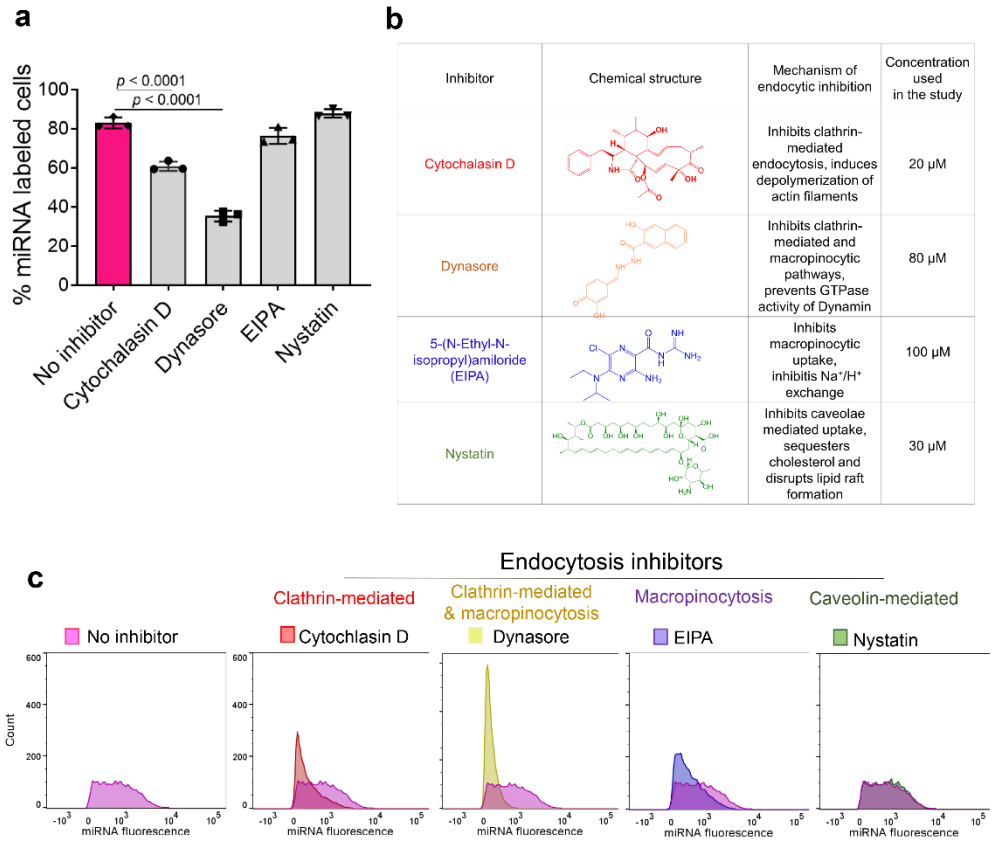

Figure S10. Mechanism of H2052 cell entry for 10:1 (N:P) particles. a, Percentage of cells labeled with FAM-miRNA at 1 h post-exposure to the nanoparticles in the presence or absence of endocytic inhibitors, Data = mean ± SD, n = 3 independent samples, representative of 2 independent experiments. Ordinary one-way ANOVA & Dunnett's multiple comparison test. **b**, Structures and functions of endocytosis inhibitors along with concentrations used. **c**, Flow cytometric histograms of cells treated with the nanoparticles for 1 h in the presence or absence of Cytochalasin D[4], Dynasore[5], EIPA[6] or Nystatin[7]. Data to accompany Figure 2l.

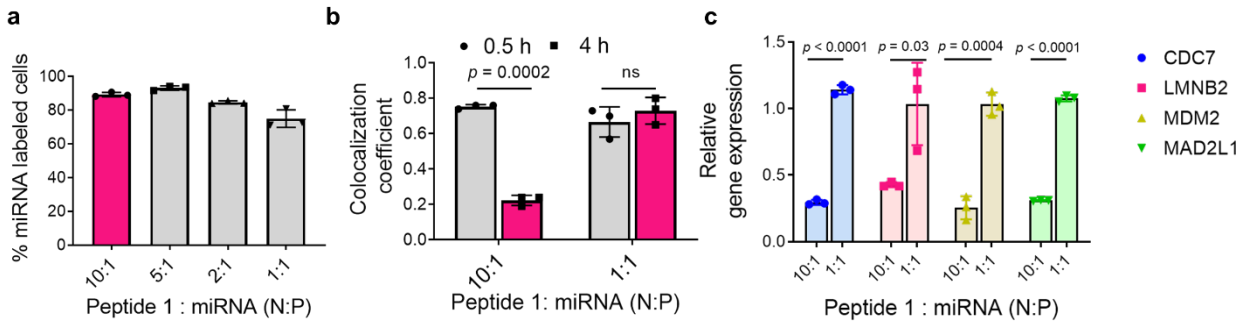

Figure S11. **miRNA cell delivery and target gene silencing efficiency as a function of Peptide 1/miRNA charge ratio**. **a**, miRNA cell delivery efficiency of nanoparticles with varying N:P ratios in H2052 cells after 1 h exposure. Data = mean ± SD, n = 3 independent samples, representative of 2 independent experiments. **b,** Colocalization of FAM-miRNA with acidic endosome marker, LysoT-red in H2052 cells treated with 10:1 and 1:1 (N:P) nanoparticles measured by fluorescence at each time point. Data = mean ± SD for n = 3 samples, representative of 3 independent experiments, two-tailed student's t test. **c**, 10:1 (N:P) nanoparticles are more effective in silencing the expression levels of the miRNA-215 target genes as compared to 1:1 (N:P) nanoparticles in H2052 cells 48 h post-treatment. Data = mean ± SD, n = 3 independent samples, representative of 3 independent experiments, two-tailed student's t test.

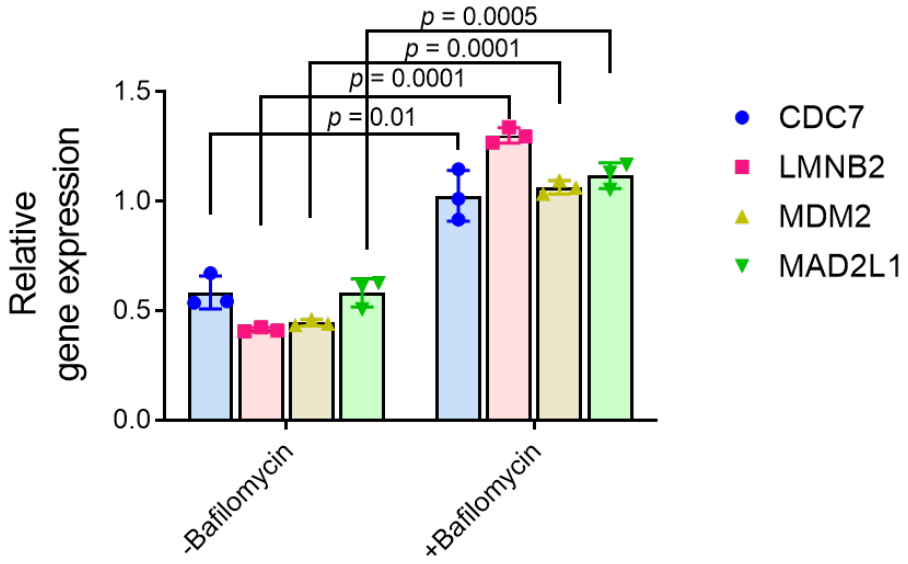

Figure S12. Target gene expression analysis in presence of endosomal acidification inhibitor shows that Peptide 1/miRNA nanoparticles facilitate endosomal escape. H2052 cells co-incubated with vacuolar ATPase inhibitor Bafilomycin A1 and Peptide 1/miRNA-215 (10:1, N:P) nanoparticles show increased expression levels of miRNA-215 target genes relative to the cells treated with the nanoparticles only. Cells were pre-treated for 1 h with 50 nM of Bafilomycin A1 followed by co-incubation with the nanoparticles for 4 h. Gene expression levels were measured 24 h post-addition of the nanoparticles. For samples with and without Bafilomycin treatment, gene expression levels for cells treated with miRNA-215 particles are normalized against those treated with scrambled miRNA particles. Data = mean ± SD, n = 3 independent samples, representative of 3 independent experiments, two-tailed student's t test.

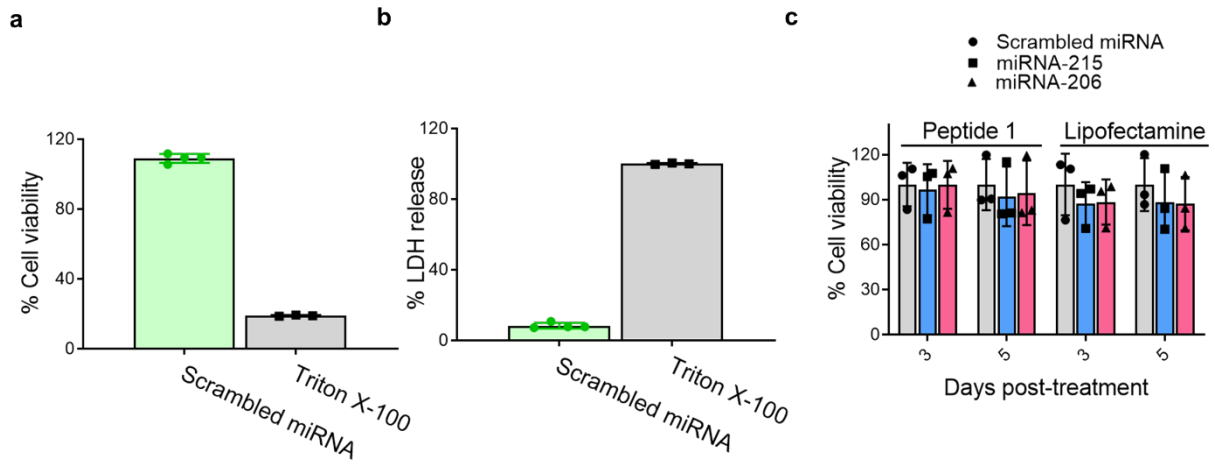

Figure S13. Peptide 1 nanoparticles formulated with scrambled miRNA are non-toxic to cancerous (H2052) cells. Peptide 1 nanoparticles formulated with scrambled, miRNA-215, or miRNA-206 are non-toxic to non-cancerous (NP4) mesothelial cells. **a**, Viability of H2052 cells treated with Peptide 1/scrambled miRNA nanoparticles 4 h post-incubation as determined by MTT assay, n = 4 independent samples for nanoparticles and n = 3 independent samples for Triton X-100. **b**, Cytotoxicity of Peptide 1/scrambled miRNA nanoparticles against H2052 cells measured by lactate dehydrogenase release 4 h post-incubation, n = 4 independent samples for nanoparticles and n = 3 independent samples for Triton X-100. In each case, Triton X-100 is a positive control. **c**, NP4 cell viability at day 3 and 5 post-treatment with the nanoparticles and lipofectamine, each delivering scrambled miRNA, miRNA-215 and miRNA-206. Data = mean ± SD, n = 3 independent experiments.

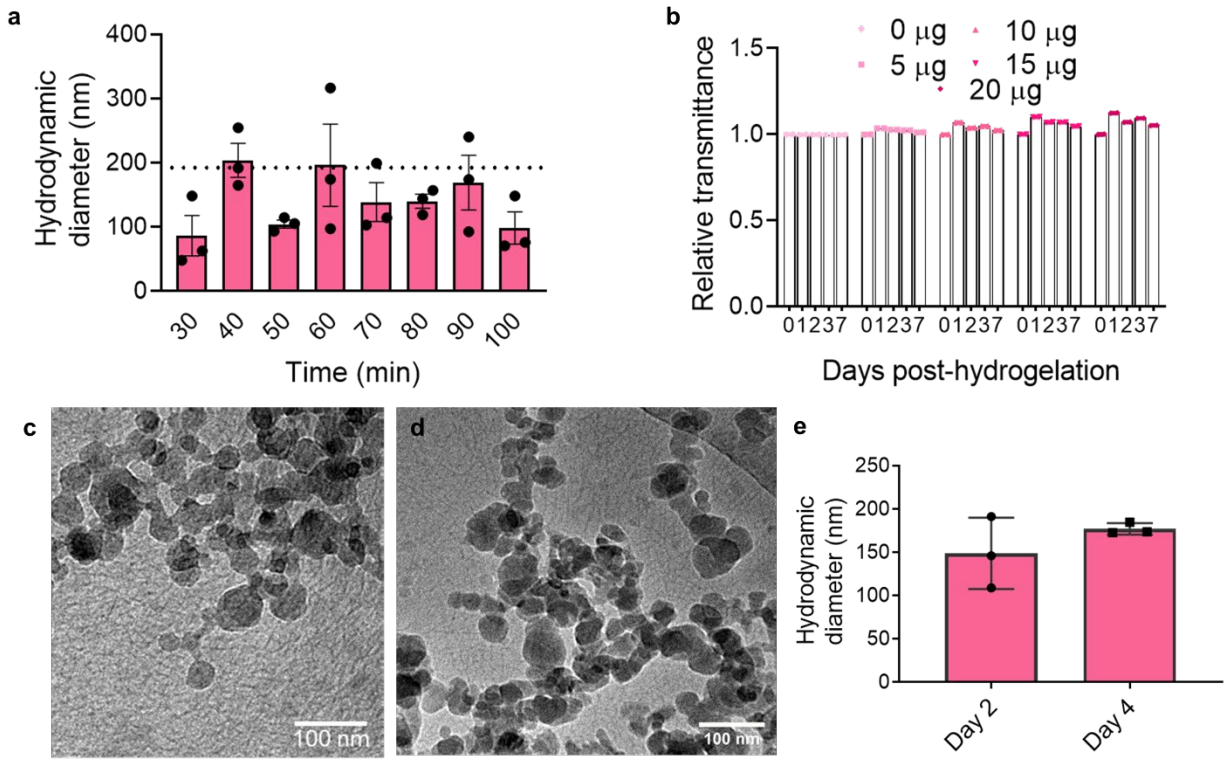

Figure S14. Stability of the nanoparticles in absence and presence of hydrogel. a, Hydrodynamic diameters of 10:1 (N:P) nanoparticles in water measured as a function of time using DLS, data = mean ± SEM for n = 3 independent samples. **b**, Transmittance of SFH stays largely unaltered when monitored for 7 days post-preparation, indicating minimal aggregation of the nanoparticles in their encapsulated state within the hydrogel matrix of SFH, irrespective of miRNA loading (5-20 μg per 100 μL of SFH). Data are shown for n = 2 independent samples. Cryo-EM of 1 wt% SFH showing miRNA nanoparticles embedded within the fibrillar gel network formed by self-assembled Peptide 3 at day 1 (**c**) and day 7 (**d**) post-preparation. Scale bar 100 nm for both panels. Uncropped micrographs (Figure S26c,d). Data are representative of 2 independent experiments. **e**, Hydrodynamic diameters of nanoparticles released from SFH at day 2 and day 4 as measured by DLS. Data are shown for n = 3 samples. Data = mean ± SD.

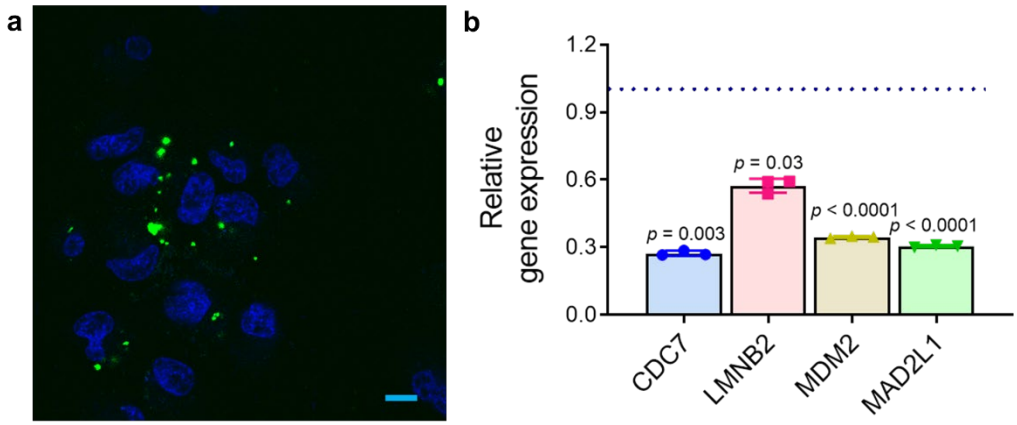

Figure S15. Biological activity of Nanoparticles released from SFH. a, Confocal micrograph of FAM-labeled scrambled-miRNA nanoparticles released from 1 wt% SFH that have entered cells. Nanoparticles released from SFH were collected at 24 h from the supernatant and incubated with cells. Image collected 4h post incubation. Cell nuclei were stained blue. Scale bar 10 μm. Data are representative of 2 independent experiments. **b**, miRNA-215 nanoparticles released from SFH effectively silence genes. Particles were collected at 24 h from the SFH and used to treat H2052 cells for 4 h. After which, the cells were assayed at 48 h. n = 3 independent samples. Data = mean ± SD. Two-tailed student's t test.

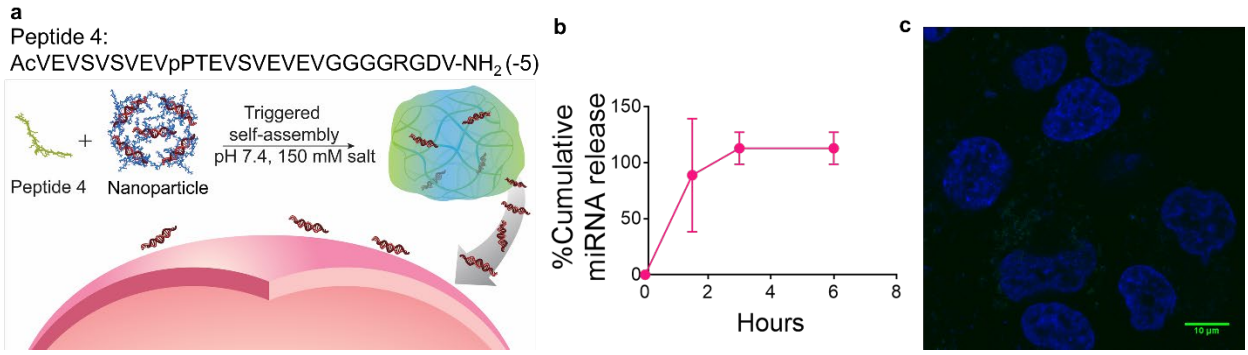

Figure S16. miRNA nanoparticles are unstable when encapsulated in a negatively charge hydrogel. a, Schematic showing the encapsulation of nanoparticles in a negatively charged hydrogel network composed of Peptide 4. The intrinsically disordered peptide 1 used to prepare the nanoparticles rapidly exchanges its binding partner, partitioning to the negatively charged fibrillar network and releasing free RNA. **b**, Rapid release of free FAM-miRNA into an infinite sink from nanoparticles that had been encapsulated in a negatively charged gel comprised of Peptide 4 (25 mM HEPES, 150 mM NaCl) at 37 ºC, n = 3 independent samples. Data = mean ± SD. In addition to releasing free miRNA, the binding of Peptide 1 to the network fibrils destabilizes the gel resulting in gel dissolution. **c**, H2052 cells treated for 4 h with supernatant collected in panel (b) after 4 h of release that contains free RNA. The lack of green fluorescence in the micrograph shows that RNA is unable to enter cells. Cell nuclei were stained blue. Data are representative of 2 independent experiments. Scale bar 10 µm.

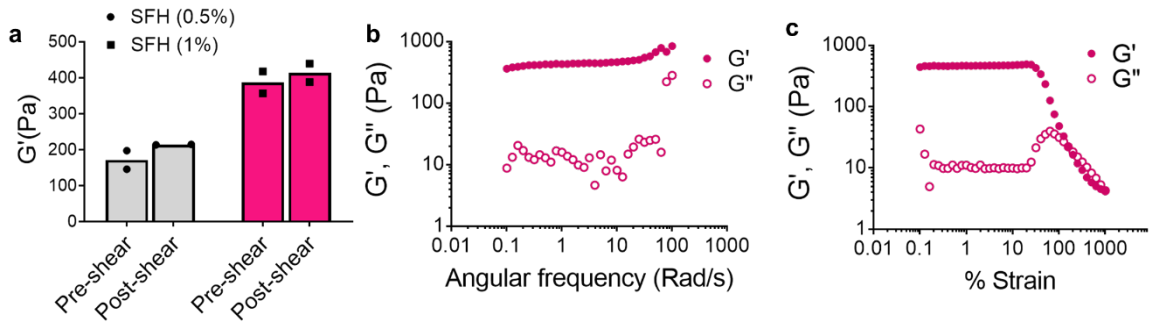

Figure S17. Rheological characterization of SFH. **a**, Plateau storage moduli (G') derived from time-sweep analysis of 0.5 and 1 wt% SFH before and after shear thinning at 1000% strain demonstrating shear-thin/recovery behavior. Data are shown for n = 2 independent samples. **b**, Oscillatory rheological frequency-sweep (0.2% strain) and (**c**) strain-sweep (6 Rad/s) of 1 wt% SFH show that the time-sweep data in Figure 4c was collected in the linear regime of both frequency and strain (0.2% strain, 6 Rad/s frequency). In these experiments, SFH was exposed to shear-thinning at 10 minutes post-initiation of the rheological study.

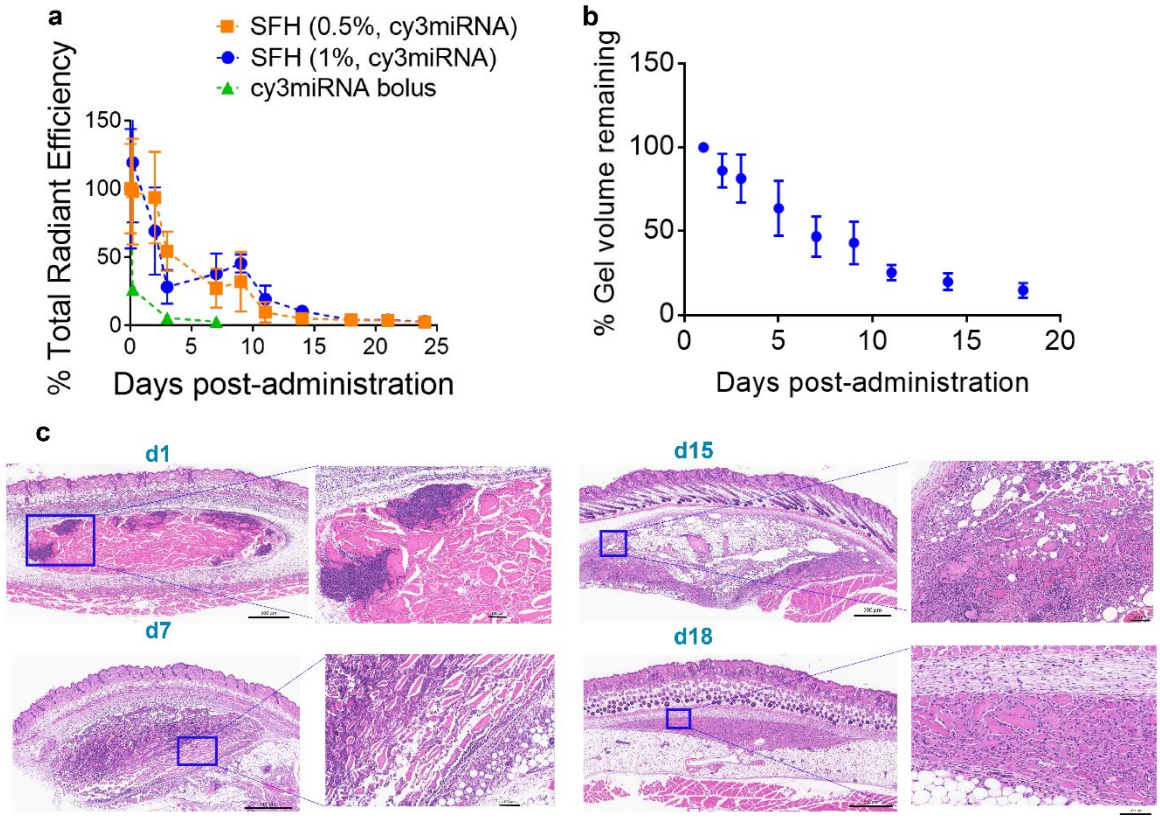

Figure S18. Quantification of in vivo release of miRNA and biodegradation of SFH. a, Quantification of cy3 miRNA level after subcutaneous injection of miRNA alone or SFH as a function of time determined by total radiant efficiency from athymic nu/nu mice as shown in Fig 5a. Radiant efficiency at each time point was normalized to day 0 for each treatment group. Data = mean ± SD for n = 3 animals for groups injected with 0.5 and 1 wt% SFH and n = 2 for animals injected with miRNA bolus. **b**, Volume of the gel implants (1 wt% SFH) measured as a function of time calculated from 3D grayscale ultrasound images using Vevo LAZR Ultrasound Imaging Software. Data = mean ± SEM for n = 3 animals. **c**, Hematoxylin and Eosin (H & E) staining of histological sections collected at different time points from mice receiving subcutaneously injected SFH to monitor SFH degradation and immune cell infiltration. Neutrophil infiltration (d1) followed by macrophage infiltration and phagocytosis mediates clearance. Data at days 1, 7, 15, and 18 are representative of 6, 5, 7, and 7 independent sections, respectively. H & E images evaluated by a board-certified veterinary pathologist are displayed at 10X (scale bar 500 μm) and 40X magnification (scale bar 100 μm). Report by the pathologist is outlined below.

Tissue: Skin and subcutis at injection site 24 hours post-injection

Acellular foreign material consistent with the injected gel is present in 3/6 sections examined. There are abundant, brightly eosinophilic (pink) fragments of acellular foreign material (consistent with the injected gel) in the subcutaneous injection site. Large numbers of neutrophils infiltrate the subcutis around this material and multifocally infiltrate the gel injection site itself. Moderate numbers of neutrophils are present throughout the hypodermis. There is moderate necrosis and

neutrophil infiltration of skeletal muscle immediately above and below the gel injection site. Few blood vessels around the gel injection site are necrotic and/or contain fibrin thrombi.

Tissue: Skin and subcutis at injection site 7 days post-injection

Acellular foreign material consistent with the injected gel is present in 3/5 sections examined. There are abundant fragments of brightly eosinophilic (pink) fragments of acellular foreign material (consistent with the injected gel) admixed with abundant necrotic neutrophilic debris. Multifocally, aggregates of macrophages surround gel fragments around the periphery of the gel injection site. There is necrosis and regeneration of the surrounding muscle.

Tissue: Skin and subcutis at injection site 15 days post-injection

Acellular foreign material consistent with the injected gel is present in 2/7 sections examined. Gel is still present but is less abundant than at day 7. Moderate numbers of neutrophils infiltrate the gel injection site, but the majority of the cells present in the area of injection are now macrophages, some of which have gel fragments in their cytoplasm (fragments were phagocytosed). Macrophages often surround gel fragments, and scattered multinucleate giant cells are present. There is minimal reactive fibroplasia of the adjacent surrounding subcutis. Peripheral nerves and blood vessels trapped in the areas of immune cell infiltration are degenerate/necrotic/inflamed. Adjacent muscle is regenerative.

Tissue: Skin and subcutis at injection site 18 days post-injection

Acellular foreign material consistent with the injected gel is present in 1/7 sections examined. The apparent area of the injection site is smaller than at 15 days post-injection. There is less gel present than was observed at 15 days post-injection. The immune cell infiltrate is almost exclusively macrophages, many of which surround the remaining gel fragments. Few neutrophils are scattered throughout the injection site. There is mild reactive fibroplasia of the subcutis over the injection site. A blood vessel within the injection site that was previously thrombosed has recanalized.

Caroline Andrews, DVM, PhD, Diplomate American College of Veterinary Pathologists

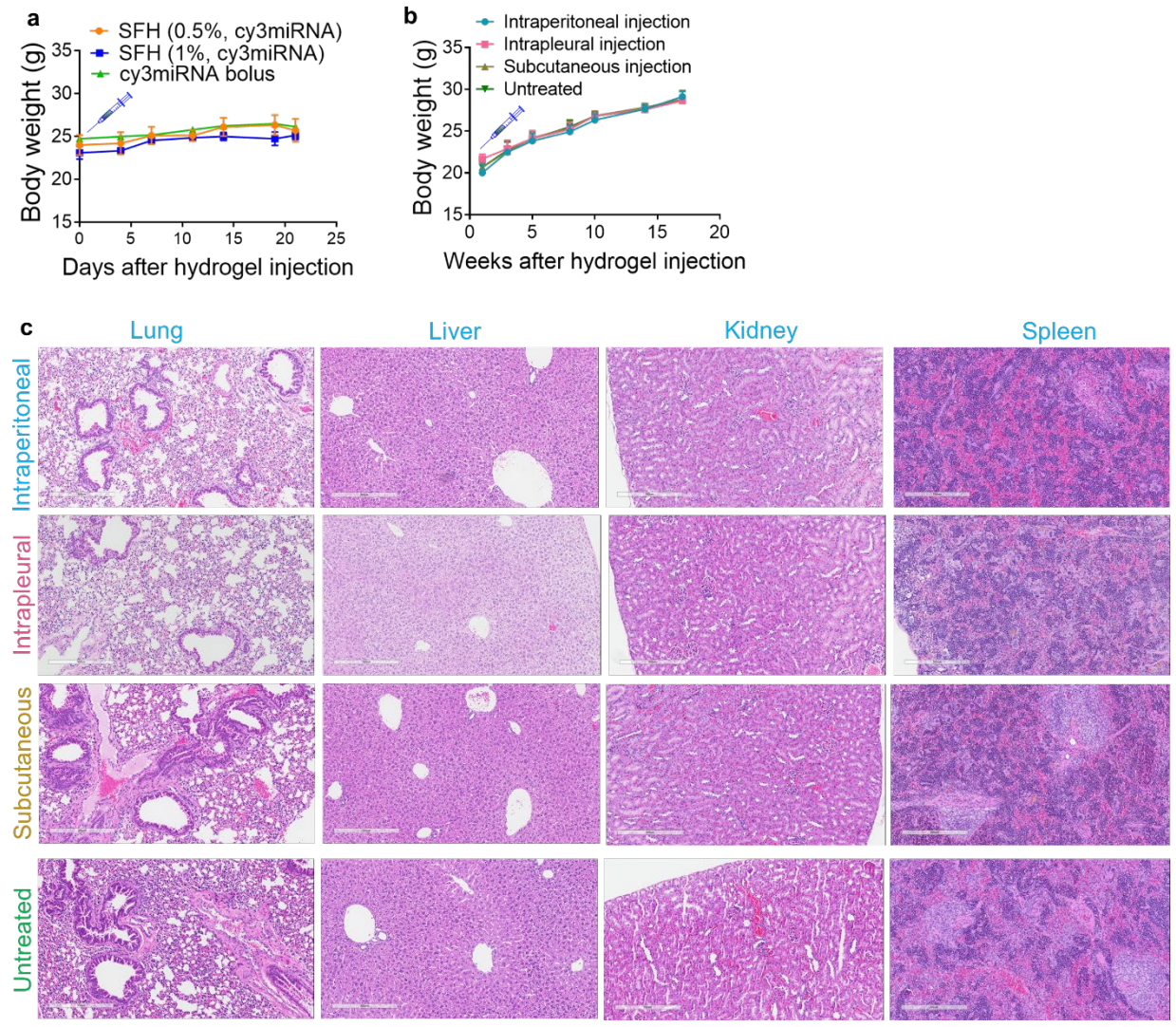

Figure S19. Biocompatibility of SFH evaluated in nu/nu mice. a, Body weights of athymic nu/nu mice receiving a single subcutaneous dose of SFH containing Cy3-miRNA nanoparticles as monitored over 3 weeks, Data = mean ± SD for n = 3 animals for groups injected with 0.5 and 1 wt% SFH and n = 2 for animals injected with miRNA bolus. **b**, Body weights of NSG mice receiving subcutaneous, intrapleural, or intraperitoneal SFH containing scrambled miRNA nanoparticles. For intrapleural, subcutaneous and intraperitoneal administrations, 100, 200 and 400 µL SFH was injected, respectively, Data = mean ± SD, n = 3 animals. **c**, H & E staining of tissue sections from vital organs of mice in corresponding treatment groups, collected after 2 months of administration of SFH, were evaluated by a Board-certified veterinary pathologist. Data representative of 2 animals.

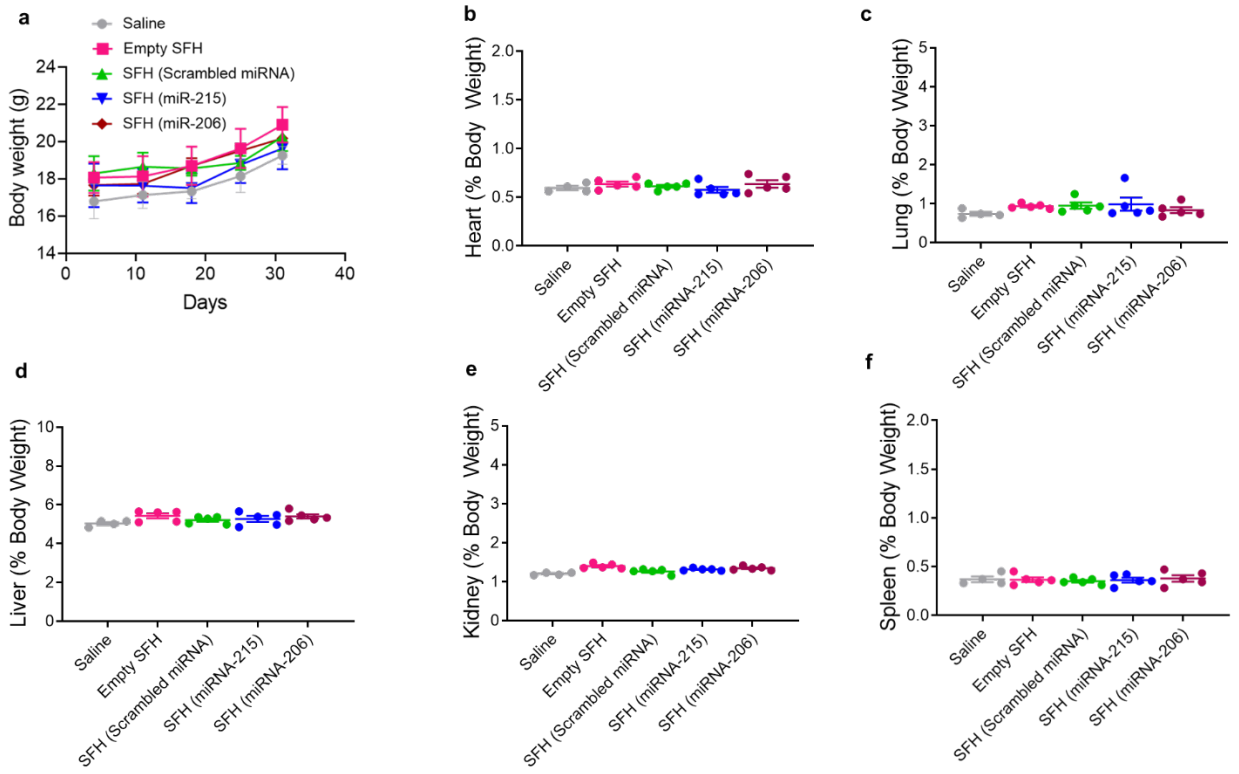

Figure S20. Biocompatibility of SFH evaluated in C57BL/6J mice. a, Body weights of mice receiving a single subcutaneous dose of empty SFH or SFH containing scrambled miRNA, miRNA-215 and miRNA-206 were monitored over 1 month. Measurements are for n = 8 mice in all groups until day 11. Measurements at days 18, 25 and 31 are 4 mice for the saline group and 5 for the remaining groups; mice were taken from the groups for accompanying studies. **b-f**, Weight of the vital organs collected from each group were normalized against the average body weight of the corresponding group. Data = mean ± SD for n = 4 animals for group injected with saline, and n = 5 animals for groups injected with SFH.

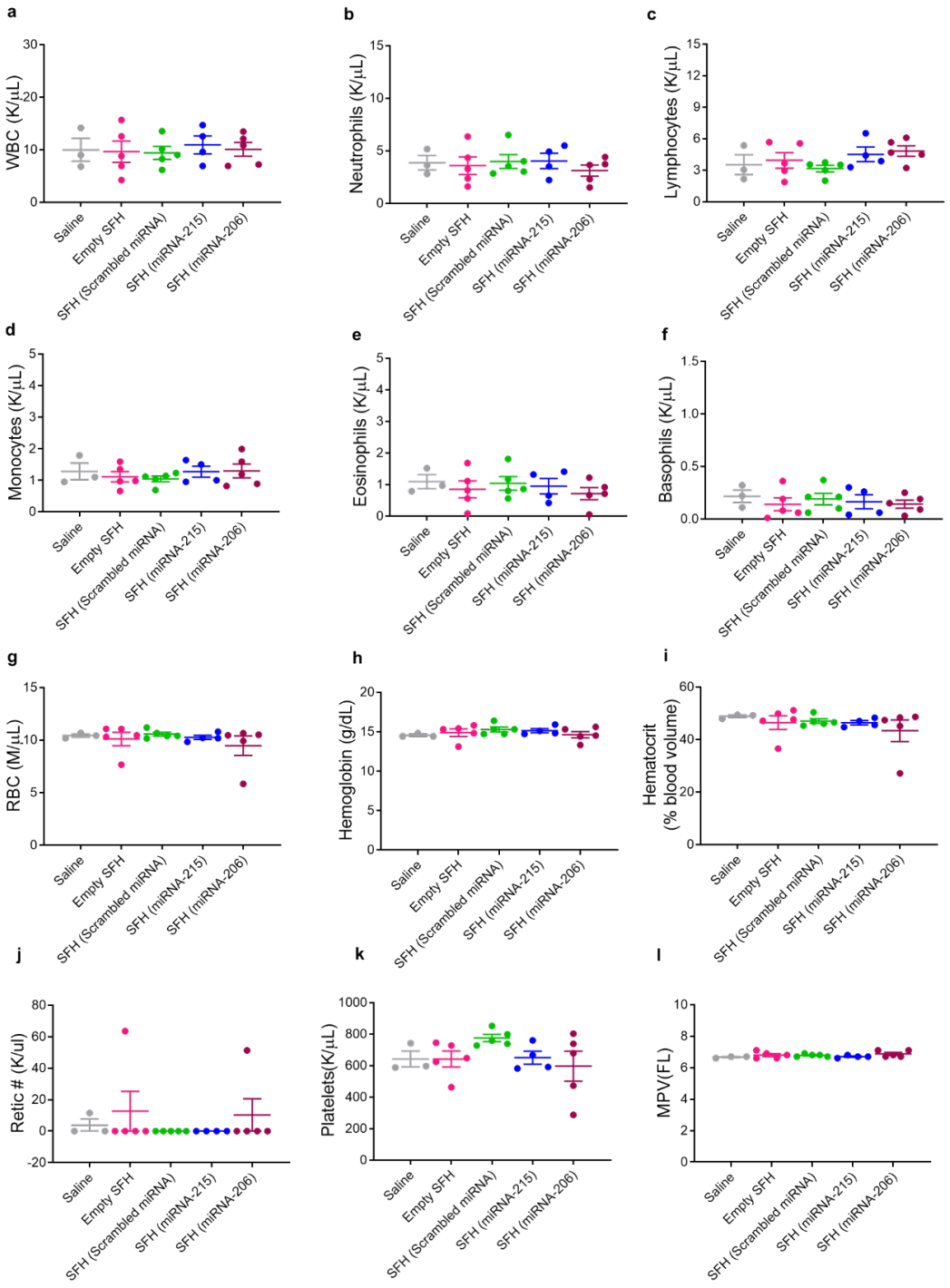

Figure S21. Safety profiles of SFH evaluated in C57BL/6J mice and determined with Complete Blood Count (CBC) analyses. Blood samples were drawn from mice at day 31 post-subcutaneous administration with saline, empty SFH or SFH containing scrambled miRNA, miRNA-215 and miRNA-206. Data = mean ± SD for n = 3 animals for group injected with saline, n = 4 for group injected with SFH (miRNA-215) and n = 5 for the rest. WBC = white blood cell; MPV = mean platelet volume(fL); RBC = red blood cell; Retic = reticulocytes.

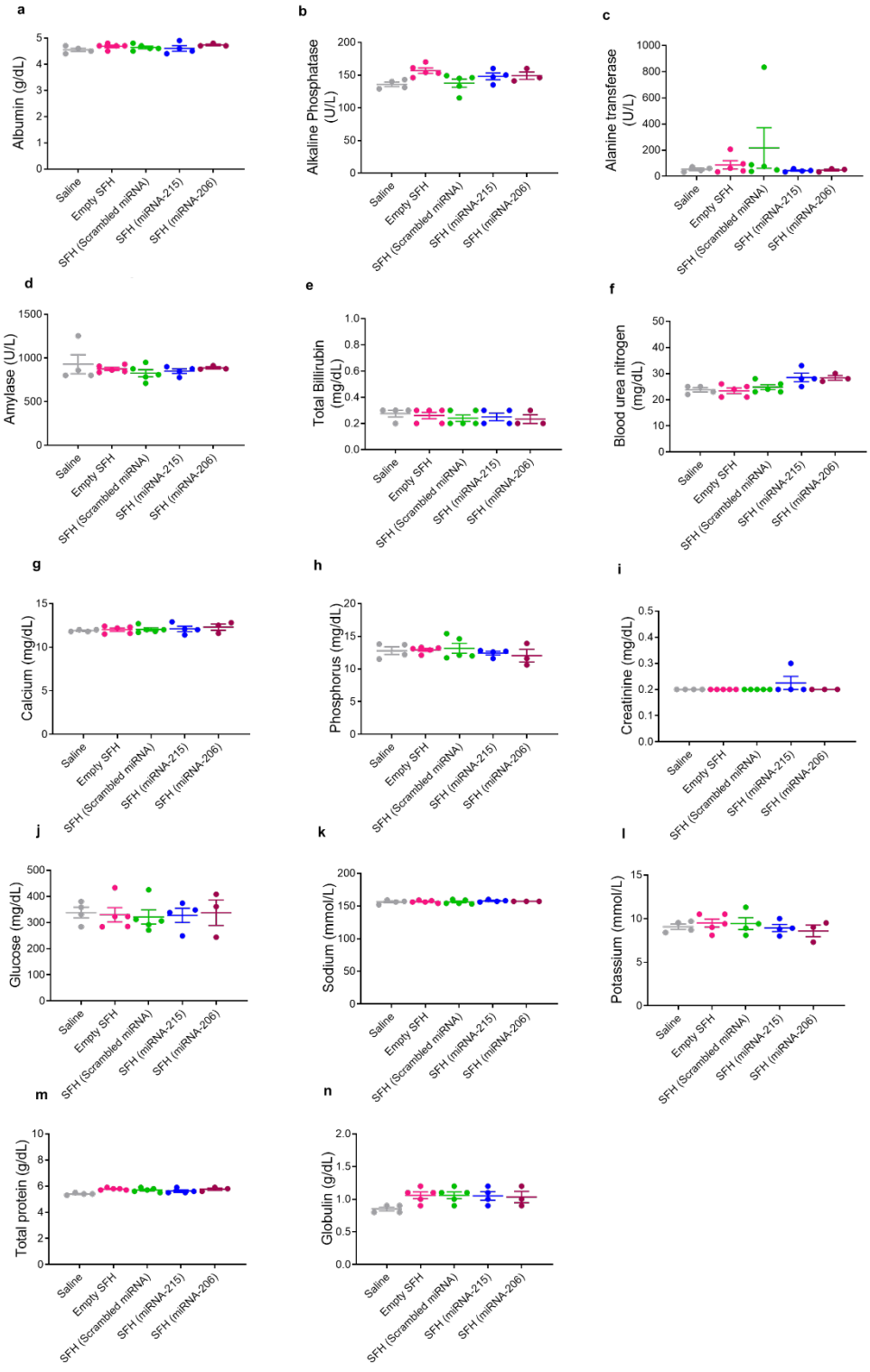

Figure S22. Safety profiles of SFH evaluated in C57BL/6J mice and determined with blood chemistry analyses. Blood samples were drawn from mice at day 31 post-subcutaneous administration with saline, empty SFH or SFH containing scrambled miRNA, miRNA-215 and miRNA-206. Data = mean ± SD for n = 4 animals for group injected with saline and SFH (miRNA-215), n = 3 for SFH (miRNA-206) and n = 5 for the rest.

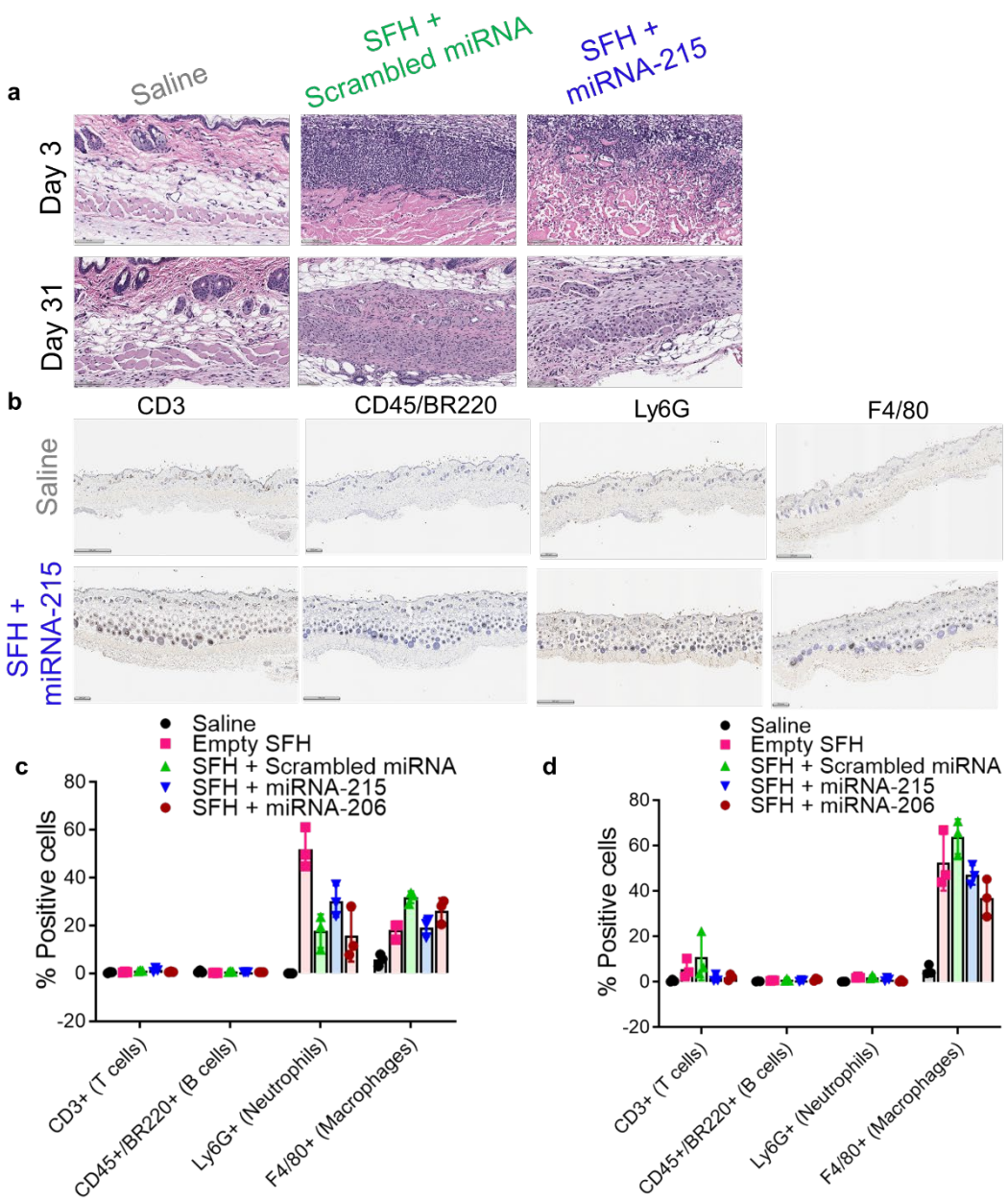

Figure S23. Safety profiles of SFH evaluated in C57BL/6J mice and determined with immunohistochemistry analyses. Tissue sections were collected from mice at day 3 and day 31 post-subcutaneous administration with saline, empty SFH or SFH containing scrambled miRNA, miRNA-215 and miRNA-206. Sections were stained with H&E and immmunostained for CD3, CD45/BR220, Ly6G and F4/80, the markers for T cells, B cells, neutrophils and macrophages, respectively. Immunostaining and quantification were performed by a Board-certified pathologist. **a**, Representative H&E stained sections collected at day 3 and day 31 from mice treated with saline, SFH + Scrambled miRNA and SFH + miRNA-215. Data are representative of n = 3 animals. **b**, Representative stained sections collected at day 31 from mice

treated with saline and SFH + miRNA-215. Data are representative of n = 3 animals. **c** & **d**, Quantification of number of positive cells at day 3 and day 31 post-treatment. Data = mean ± SD for n = 3 animals. Report by the pathologists is outlined below.

At day 3 post injection, hydrogel is observed in both (SFH + miRNA-215) and (SFH + scrambled miRNA). There is a nodular aggregate of brightly eosinophilic, amorphous hydrogel material expanding the subcutaneous adipose tissue. Present within the margin of this nodular aggregate and surrounding connective tissue, there is a high number of inflammatory cells composed of neutrophils with occasional mononuclear cells. At day 31 post injection, the implanted gel in both groups; SFH + miRNA-215 and SFH + scrambled miRNA has been reabsorbed and the site is replaced by macrophages with intracytoplasmic, eosinophilic, amorphous, phagocytosed hydrogel. No specific histologic findings are recognized within samples from animals that received saline injections.

Albert Jeon, DVM, PhD

Baktiar Karim, DVM, PhD

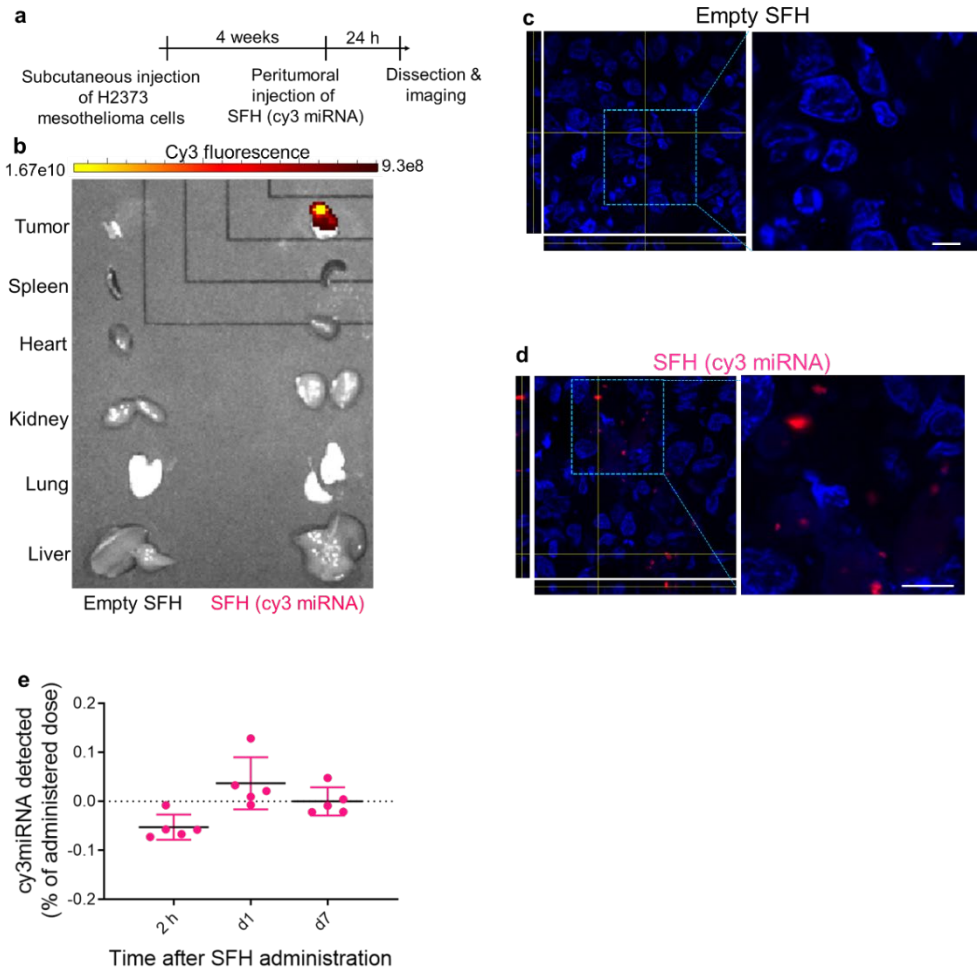

Figure S24. Peritumoral injection of SFH delivers miRNA locally to cells. a, SFH containing Cy3-labelled miRNA was injected peritumorally at 4 weeks post-tumor inoculation to NSG mice bearing subcutaneous H2373 xenografts. Tumors and vital organs were collected 24 h post-injection of 1 wt% SFH for imaging cy3 fluorescence in an IVIS Xenogen imaging system. **b**, Analysis of miRNA biodistribution in tumors and vital organs collected 24 h post-injection of SFH by measuring cy3 fluorescence signal. Corresponding images from a control mouse receiving empty SFH at the same time are also shown. **c**, Representative confocal micrographs of tumor section derived from mice injected with empty SFH. Data representative of 2 independent experiments. **d**, Similar micrographs of tumor section derived from mice receiving peritumoral injections of SFH containing cy3-labelled nanoparticles. Nuclei are stained blue (DAPI). Corresponding z-stacks are also shown. Scale bar 10 µm. Absence of fluorescence signal in tumor sections collected from mice injected with blank hydrogel rules out the possibility of tumor tissue autofluorescence. Data representative of 2 independent experiments. **e**, Time-dependent fluorescence determination of plasma levels of cy3-labelled miRNA delivered from subcutaneously implanted SFH. Y-axis indicates cy3-labelled miRNA fluorescence relative to background serum fluorescence obtained from mice receiving miRNA-free (empty) SFH. Data indicates miRNA delivered by SFH does not enter systemic circulation. Data = mean ± SD for n = 5 animals.

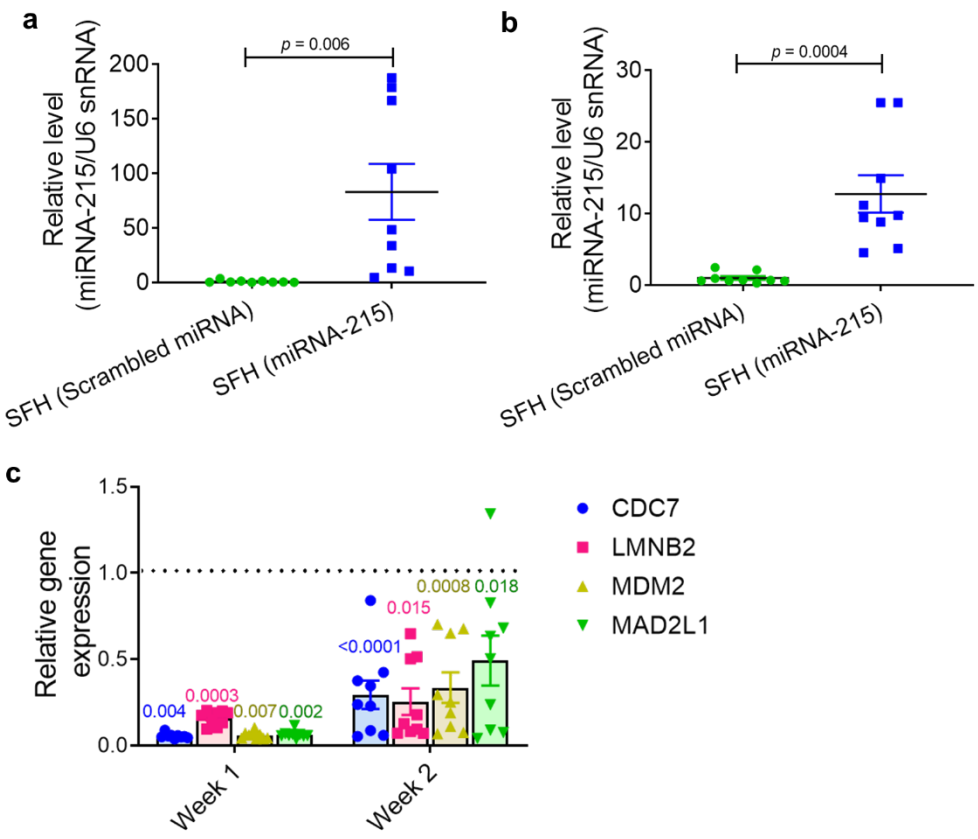

Figure S25. qPCR showing *in vivo* transfection of functional miRNA-215. **a**,**b**, Relative levels of miRNA-215 in tumor tissue resected from mice bearing H2373 mesothelioma subcutaneous xenograft at week 1 and week 2, respectively. Tumor bearing control animals received SFH containing scrambled miRNA. miRNA levels are normalized to U6 snRNA. Data = mean ± SEM for n = 3 mice per group, 3 sections of each mouse xenograft were measured, two-tailed student's t test. **c**, Expression profiles of target genes in tumor tissue at week 1 and week 2 post-SFH administration. Data = mean ± SEM for n = 3 mice per group, 3 sections of each mouse xenograft were measured, two-tailed student's t test.

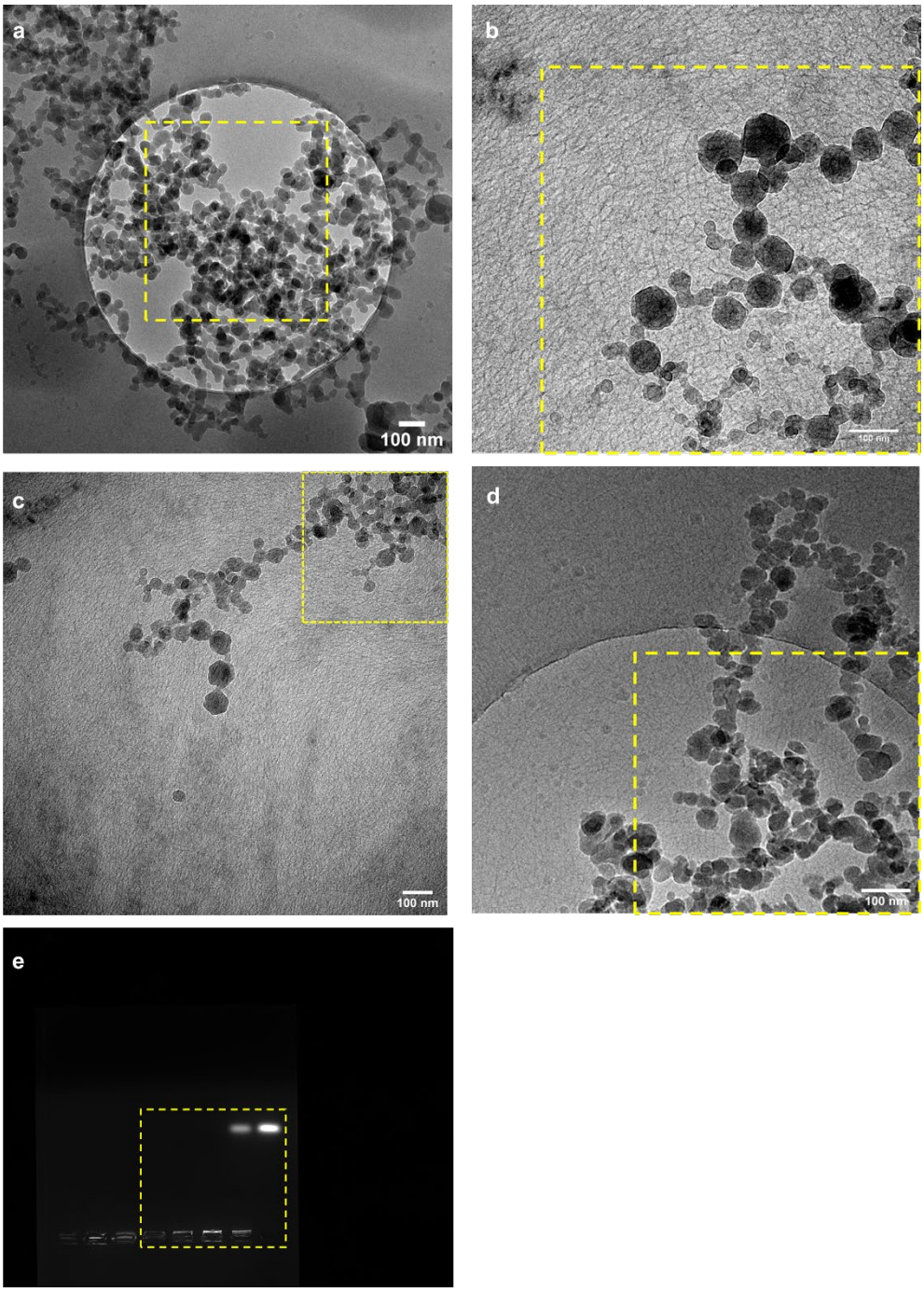

Figure S26. Uncropped cryo-EM and gel electrophoresis images. **a**, Cryo EM of 1:1 (N:P) nanoparticles, corresponding to Figure 2j. **b & c**, Cryo EM of SFH at day 1 post-preparation, corresponding to Figures4a and S14c, respectively. **d**, Cryo EM of SFH at day 7 post-preparation, corresponding to Figure S14d. **e**, Agarose gel electrophoresis assay of the nanoparticles, corresponding to Figure S4b. Yellow dashed box marks the borders of the final cropped images.

miRNA name	Catalog #	Assay ID
hsa-miR-206	4464070	MC10409
hsa-miR-215-5p	4464066	MC10874
mmu-miR-215-5p	4464066	MC10296
mirVana™ miRNA Mimic, Negative Control #1	4464061	-
FAM™-labeled Pre-miR™ Negative Control #1	AM17121	-
Cy3™ Dye-Labeled Pre-miR Negative Control #1	AM17120	-

Table S1. Details of miRNAs used in the study. Each of these were purchased from Thermo Fisher Scientific.

TaqMan® assay probe for	Catalog #/Assay ID
miR-215-5p	478516_mir
miR-206	477968_mir
U6 snRNA	TM 001973
MDM2	Hs004999839_m1
MAD2L1	Hs01554513_g1
CDC7	Hs00177487_m1
LMNB2	Hs00383326_m1
KRAS	Hs00364284_g1
CDK4	Hs00364847_m1
CCND1	Hs00765553_m1
MET	Hs01565584_m1
β-Actin	Hs99999903_m1

Table S2. Details of TaqMan® assay probes used in the study for qPCR analyses. Each of these were purchased from Thermo Fisher Scientific.

Supplementary References

1 Phelps, R. M. *et al.* NCI-Navy Medical Oncology Branch cell line data base. *J Cell Biochem Suppl* **24**, 32-91, doi:10.1002/jcb.240630505 (1996).
2 Rintoul, R. C., Rassl, D. M., Gittins, J., Marciniak, S. J. & Mesoban, K. c. MesobanK UK: an international mesothelioma bioresource. *Thorax* **71**, 380-382, doi:10.1136/thoraxjnl-2015-207496 (2016).
3 Pruett, N., Singh, A., Shankar, A., Schrump, D. S. & Hoang, C. D. Normal mesothelial cell lines newly derived from human pleural biopsy explants. *Am J Physiol Lung Cell Mol Physiol* **319**, L652-L660, doi:10.1152/ajplung.00141.2020 (2020).
4 Lamaze, C., Fujimoto, L. M., Yin, H. L. & Schmid, S. L. The actin cytoskeleton is required for receptor-mediated endocytosis in mammalian cells. *J Biol Chem* **272**, 20332-20335 (1997).
5 Kirchhausen, T., Macia, E. & Pelish, H. E. Use of dynasore, the small molecule inhibitor of dynamin, in the regulation of endocytosis. *Methods Enzymol* **438**, 77-93, doi:10.1016/S0076-6879(07)38006-3 (2008).
6 Koivusalo, M. *et al.* Amiloride inhibits macropinocytosis by lowering submembranous pH and preventing Rac1 and Cdc42 signaling. *J Cell Biol* **188**, 547-563, doi:10.1083/jcb.200908086 (2010).
7 Chen, Y. *et al.* Cholesterol sequestration by nystatin enhances the uptake and activity of endostatin in endothelium via regulating distinct endocytic pathways. *Blood* **117**, 6392-6403, doi:10.1182/blood-2010-12-322867 (2011).